Geological Survey of Canada

CURRENT RESEARCH
2004-F2

Temporal relationships between plutonism, metamorphism, and gold mineralization in southwestern New Brunswick: U-Pb and $^{40}Ar/^{39}Ar$ geochronological constraints

William J. Davis, Guoxiang Chi,
Sébastien Castonguay, and Malcom McLeod

2004

CURRENT RESEARCH

Natural Resources Canada Ressources naturelles Canada

Canada

ISSN 1701-4387
Catalogue No. M44-2004/F2E-PDF
ISBN 0-662-38132-7

A copy of this publication is also available for reference by depository libraries across Canada through access to the Depository Services Program's website at http://dsp-psd.pwgsc.gc.ca

A free digital download of this publication is available from the Geological Survey of Canada Bookstore web site:

http://gsc.nrcan.gc.ca/bookstore/

Click on Free Download.

Authors' addresses

W.J. Davis (bidavis@nrcan.gc.ca)
Continental Geoscience Division
Geological Survey of Canada
601 Booth Street
Ottawa, ON K1A 0E8

G. Chi (guoxiang.chi@uregina.ca)
Department of Geology
University of Regina
Regina, SK S4S 0A2

S. Castonguay (scastong@nrcan.gc.ca)
GSC-Québec
880 chemin Sainte-Foy
Québec, QC G1S 2L2,

M. McLeod (Malcolm.McLeod@gnb.ca)
New Brunswick Geological Survey
207 Picadilly Rd.
Sussex, NB E4E 5L2

Publication approved by CGD

Temporal relationships between plutonism, metamorphism, and gold mineralization in southwestern New Brunswick: U-Pb and $^{40}Ar/^{39}Ar$ geochronological constraints [1]

William J. Davis, Guoxiang Chi, Sébastien Castonguay, and Malcom McLeod

Davis, W.J., Chi, G., Castonguay, S., and McLeod, M., 2004: Temporal relationships between plutonism, metamorphism, and gold mineralization in southwestern New Brunswick: U-Pb and 40Ar-39Ar geochronological constraints; Geological Survey of Canada, Current Research 2004-F2, 20 p.

Abstract: New U-Pb and $^{40}Ar/^{39}Ar$ dates from plutonic rocks and quartz veins associated with gold occurrences in southwestern New Brunswick provide timing constraints for mineralization. Plutonic rocks spatially associated with economically significant gold mineralization are all Early Devonian, including a microgranite dyke near the Tower Hill pluton (409 ± 2.4 Ma), the Jimmy Hill granite (403 ± 2 Ma), and a granitic dyke at the Clarence Stream main zone (395.5 ± 0.5 Ma). An auriferous pegmatite dyke at Clarence Stream has a maximum age of ~400 Ma based on inherited zircon. Muscovite from quartz veins at the Clarence Stream main zone yields $^{40}Ar/^{39}Ar$ ages of 395.5 ± 3.6 Ma to 388.9 ± 3.6 Ma and provides minimum age estimates for gold mineralization. The close spatial and temporal association of gold mineralization with Devonian plutonism is consistent with a genetic link.

Résumé : De nouvelles datations U-Pb et $^{40}Ar/^{39}Ar$ de roches plutoniques et de filons de quartz associés à des indices aurifères dans le sud-ouest du Nouveau-Brunswick permettent d'encadrer l'âge de la minéralisation. Toutes les roches plutoniques associées dans l'espace à une minéralisation aurifère d'importance économique remontent au Dévonien précoce, y compris un dyke microgranitique près du pluton de Tower Hill (409 ± 2,4 Ma), le granite de Jimmy Hill (403 ± 2 Ma) et un dyke granitique de la zone principale de la propriété Clarence Stream (395,5 ± 0,5 Ma). Un dyke de pegmatite aurifère sur la propriété Clarence Stream a un âge maximal d'environ 400 Ma, d'après la datation de zircons hérités. De la muscovite provenant de filons de quartz dans la zone principale de la propriété Clarence Stream donne des âges $^{40}Ar/^{39}Ar$ qui s'échelonnent de 395,5 ± 3,6 Ma à 388,9 ± 3,6 Ma et fournit des estimations de l'âge minimal de la minéralisation aurifère. L'étroite association spatio-temporelle entre la minéralisation aurifère et le plutonisme dévonien indiquerait l'existence d'un lien génétique.

[1] Contribution to the Targeted Geoscience Initiative (TGI) 2000–2003

INTRODUCTION

Recent research (e.g. McLeod and McCutcheon, 2000; Chi et al., 2001; Thorne and Lentz, 2001; Thorne et al., 2002a; Chi, 2002, Castonguay et al., 2003; Thorne and McLeod, 2003a; Watters et al, 2003) and exploration work highlight the potential for intrusion-related gold systems in southwestern New Brunswick. Many of the southwestern New Brunswick gold occurrences are comparable to the intrusion-related gold systems found in the Tintina Belt of Alaska and the Yukon Territory (*see* Lang and Baker, 2001 for a review), and a similar exploration model may apply. One of the key requirements to assess the validity of this exploration model is establishing a direct temporal link between potential progenitor intrusions and mineralization.

The granite-dominated districts of southwestern New Brunswick are best known for their W-Sn-Mo-Sb resources, including the former major antimony and tungsten producers at Lake George and Mount Pleasant (Fig. 1a). Gold mineralization, including the two most significant occurrences at Poplar Mountain and Clarence Stream, occurs near two large granitoid bodies, the Devonian Pokiok and Siluro-Devonian Saint George batholiths, respectively (Fig. 1a). However, unlike the W-Sn-Mo-Sb mineralization, the temporal and genetic relationships between gold mineralization and granitic intrusions have not been firmly established. In this report U-Pb results for igneous intrusions and $^{40}Ar/^{39}Ar$ dates for mineralized veins and metamorphic minerals spatially associated with gold mineralization on the northwestern side of the St. George Batholith are presented (Fig. 1b). The results support recent proposals that significant gold mineralization in the region is both spatially and temporally related to Early Devonian plutonism (e.g. Seal et al. 1988; McLeod, 1990).

GEOLOGICAL SETTING

The study area straddles three of the major tectonostratigraphic belts (Fyffe and Fricker, 1987; Williams, 1995; Fyffe et al. 1999; New Brunswick Department of Natural Resources and Energy, 2000) that constitute the New Brunswick segment of the northern Appalachians. (Fig. 1b). The Late Cambrian to Ordovician St. Croix Terrane (composed mostly of the Cookson Group), traditionally assigned to the Gander Zone, is flanked on both sides by cover sequences along unconformable and/or faulted contacts: the Silurian Fredericton Belt (Kingsclear Group) to the northwest, and the Late Ordovician to Early Devonian Mascarene Belt (Mascarene Group), southeast of the Sawyer Brook Fault. The latter is interpreted as the boundary between the St. Croix and peri-Gondwanan terranes.

The regional structural geology of the area is characterized by four main phases of deformation (D_1–D_4) that vary in style and intensity due to differences of rock competency and anisotropy (Ruitenberg, 1967; Castonguay et al., 2003). Deformation related to the D_1 and D_2 events has produced thrust faults and fault-related folds, which mainly affect the St. Croix Terrane and part of the Fredericton Belt, and are considered to be related to a protracted compressive and northwest-directed thrusting of the St. Croix Terrane onto the Fredericton Belt in Late Silurian–Early Devonian (Ludman, 1991). D_3 structures are regionally developed, but are dominant in the Late Silurian strata of the Mascarene Belt. They consist mainly of steeply plunging tight folds with axial-planar, steeply dipping fabric cut by dextral strike-slip faults (Castonguay et al., 2003), which may be related to the Acadian Orogeny that culminated in the Middle Devonian. D_4 deformation has produced late chevron folds and is likely post-Acadian, perhaps Alleghanian or as late as Mesozoic. The St. David Antiform (St. David Dome of Ruitenberg, 1967), an important structure in the area, is interpreted as a megascopic F_2-F_3 fold interference structure (Castonguay et al., 2003), the southeast limb of which is cut by the late-D_3 dextral Sawyer Brook fault, which juxtaposes the Silurian Mascarene Group against units of the Ordovician Cookson Group (Fig 1b).

Several Late Silurian to Late Devonian granitoid intrusions occur in the area (Fig. 1b; e.g. Ruitenberg, 1967; McLeod et al., 1994), most of which are included in the main body of Saint George Batholith, and related satellite stocks. McLeod (1990) subdivided the intrusive rocks into five suites: 1) the Welsford Intrusive Suite (422 ± 1 Ma U-Pb), 2) the Digdeguash Lake Intrusive Suite (418 ± 5 Ma $^{40}Ar/^{39}Ar$), 3) the South Oromocto Lake Intrusive Suite (Magaguadavic granite: 396 ± 1 Ma U-Pb, 384 ± 7 Ma $^{40}Ar/^{39}Ar$), 4) the Mount Douglas Intrusive Suite (ca. 367 Ma U-Pb and $^{40}Ar/^{39}Ar$), and 5) the Pomeroy Suite (ca 360 Ma $^{40}Ar/^{39}Ar$) (includes the satellite McDougall Brook, True Hill, Beech Hill, and Kedron stocks). Uranium-lead geochronological data are reported in Bevier (1989, 1990) and Ar-Ar ages in McLeod et al. (1988), McLeod (1990), Sinclair et al. (1988), and Taylor (1992) The satellite plutons of the Pomeroy Suite and the Mount Douglas Granite are mostly highly evolved granites that generated the Mount Pleasant W-Mo-Sn-polymetallic deposits and other localized tin-bearing systems (e.g. Taylor 1985, Sinclair et al. 1988). Gravity data indicate that intrusions are present beneath much of the area at relatively shallow depths (Thomas and Willis 1989).

The regional metamorphic grade is generally lower greenschist facies (chlorite zone) (Ruitenberg, 1967; Castonguay et al., 2003). Locally higher grade rocks or hornfels (cordierite-muscovite-biotite grade, locally up to sillimanite grade) occur in contact zones around intrusions.

LOCAL GEOLOGY, SAMPLING AND ANALYTICAL RESULTS

A number of gold occurrences have been reported in the study area (McLeod, 1990; McLeod and Fyffe, 2002; Thorne and McLeod, 2003a; Watters et al., 2003). The most significant occurrences have been interpreted to be genetically related to Early Devonian granites near Clarence Stream, Jimmy Hill, and Tower Hill (Fig. 1b), while some other minor occurrences are thought to be genetically related to granites of the Late Devonian Pomeroy Suite, such as those near Kedron Stream and McDougall Brook. New geochronological

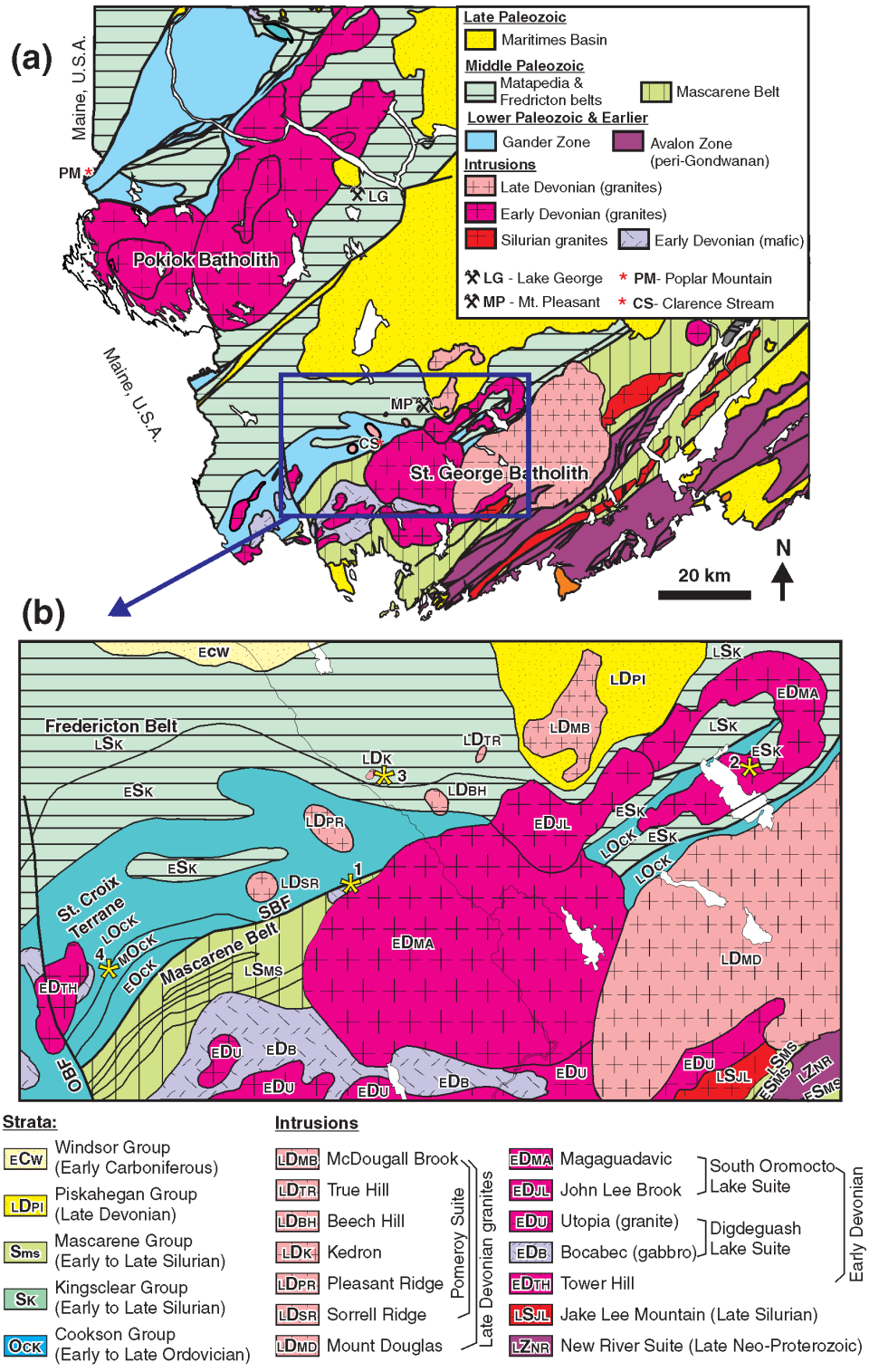

Figure 1. a) *Geological map of southwestern New Brunswick, showing the distribution of major tectonostratigraphic units and granite batholiths, the mines of Lake George and Mount Pleasant, and two of the more important gold occurrences in the region (Clarence Stream and Poplar Mountain) (modified from New Brunswick Department of Natural Resources and Energy, 2000).* ***b)*** *Enlargement of a part of (a) showing the various components of the St. George Batholith, the major stratigraphic units on the northwestern side of the batholith, and the localities of study areas. SBF: Sawyer Brook Fault; OBF: Oak Bay Fault.*

studies have been carried out at four of these gold occurrences (Clarence Stream, Jimmy Hill, Kedron, and Tower Hill; *see* Fig. 1b), and the local geology, samples, and age interpretations are described below. Uranium-lead and $^{40}Ar/^{39}Ar$ analytical methods are described in Appendix 1, and analytical data presented in Tables 1 to 3.

Jimmy Hill gold occurrence

The Jimmy Hill gold occurrence is hosted in the hornfelsed Silurian wacke of the Kingsclear Group (Digdeguash Formation) about 400 m from the contact zone with the granitic intrusion assigned to the Magaguadavic phase of the South Oromocto Lake Intrusive Suite (McLeod, 1990; Fyffe and Brown, 1996; Fig. 1b). Mineralization occurs as quartz veins up to 25 cm wide and stockworks zones with random orientations. Visible gold occurs in the veins along with wolframite, bismuthinite, arsenopyrite, molybdenite, pyrite, chalcopyrite, galena, and sphalerite. Sample GC01-146 is a massive, biotite-bearing granite containing large K-feldspar phenocrysts. It was collected from an outcrop southwest of the Jimmy Hill occurrence (Locality 2 in Fig. 1b). The sampled granite is not directly related to mineralization at this locality, but is characteristic of the granitoid phase spatially close to the Jimmy Hill occurrence.

U-Pb results: GC01-146

Zircons from the sample are clear, colourless, prismatic grains. Six analyses of multigrain fractions were carried out (Table 1). Two of the analyses (no. 5 and 6) include significant inheritance of older zircon, and have discordant $^{207}Pb/^{206}Pb$ ages of 429 and 445 Ma (Fig. 2a). Four analyses (no. 1–4) have overlapping, slightly discordant $^{207}Pb/^{206}Pb$ ages that yield an upper intercept age of 403 ± 2 Ma (forced zero lower intercept; MSWD =0.26), interpreted as the crystallization age of the pluton. Analyses of titanite yield imprecise ages, owing to significant common Pb corrections that are indistinguishable from the zircon age. The 403 ± 2 Ma age for the Jimmy Hill granite is older than a previously reported age of 396 ± 1 Ma for a Magaguadavic granite sample (U-Pb; Bevier 1990), and indicates that the intrusion is likely composite, with intrusive pulses spanning at least 7 Ma.

Kedron gold occurrence

The Kedron gold occurrence is located near the contact zone between a small cupola (about 100 m in diameter) of the Kedron pluton and hornfelsed sandstone and siltstone in the Kingsclear Group of the Fredericton Belt (Locality 3, Fig. 1b). Mineralization occurs in fluorite-bearing quartz veins and stockworks in greisenized and chloritized hornfels peripheral to the intrusion, and in a metal-rich chlorite lode (replacement body) within the granite very similar to those at the Mount Pleasant mine (Thorne and McLeod, 2003b). The analyzed sample was collected from drill core in a relatively homogeneous muscovite-bearing granite from a hole collared by Billiton Canada Limited in 1984 (BR84-4).

U-Pb results: Kedron 01

Zircon recovery was extremely poor and no zircon analyses were carried out. The sample contained monazite, typically discoloured and altered, and abundant thorite. Analyses of three of the best optical-quality monazite grains indicate extremely low U contents, and extremely high Th/U ratios (~180–280), atypical of magmatic monazite (Table 1; no. 9–11). The generally poor quality and alteration of the grains is indicated by the relatively high common Pb contents of the analyzed grains, which are well above values typical of igneous monazite. The U-Pb ages are reversely discordant, plotting above the concordia with overlapping $^{207}Pb/^{235}U$ ages of 312 to 323 Ma (Fig. 2b). Relatively large errors in the $^{207}Pb/^{235}U$ ratios result from large common Pb corrections and low total radiogenic Pb in the monazites. Assuming the reverse discordance in the $^{206}Pb/^{238}U$ age is entirely explained by initial isotopic disequilibrium (e.g. Scharer 1984), the three analyses yield a weighted mean $^{207}Pb/^{235}U$ age of 313 ± 5 Ma (MSWD = 0.82). It is unclear exactly what this date represents, especially considering the ca 362 Ma $^{40}Ar/^{39}Ar$ date reported by Taylor (1992). Based on the Th-U-Pb chemistry of the monazites, it is not interpreted as the crystallization age, but may indicate a period of alteration or metasomatism that affected the sample at ca. 313 Ma. A single analysis of thorite (no.12) was carried out and yielded a discordant result with a $^{206}Pb/^{238}U$ age of 30 Ma. The very young age of the thorite indicates that this mineral has not quantitatively retained radiogenic Pb.

Tower Hill Area

Significant gold mineralization has been documented west of the Tower Hill Granite (Locality 4, Fig. 1b; Ruitenberg, 1967, 1972) within siliceous siltstone and black shale of the Cookson Group (Thorne and Ravenelle, 2003). The Tower Hill Granite consists of a medium- to coarse-grained, biotite-muscovite-bearing granite previously dated at 401 ± 4 Ma (isochron Rb-Sr age on muscovite; Whalen et al., 1996). A sample (02SC-055) from a silicified, foliated microgranite dyke that intrudes the polydeformed host rocks was taken in an exploration trench 2 km east of the mapped contact of the Tower Hill Granite (Freewest Resources Canada Inc. Black Fly Trench 2). The highest gold concentration within the trench (3157 ppb over 1 m) is associated with arsenopyrite-bearing quartz veins within the microgranite dyke. The relationship between the microgranite and the Tower Hill Granite is not known at this time, but field observations indicate that the dyke is the youngest, premineralization rock, and thus offers the best constraint on a maximum age for mineralization.

U-Pb results: 02-SC-055

Zircons in the sample constitute a homogenous population of small prismatic crystals. Three multigrain analyses yield concordant dates with a weighted mean $^{206}Pb/^{238}U$ age of 409 ± 2.4 Ma (MSWD= 1.4), which is interpreted as the crystallization age of the dyke (Table 1; Fig. 2c). This age is generally similar to, but slightly older than, the previously reported

Table 1. U-Pb TIMS data.

Fraction[1]	Description**	No. of grains	Wt. ug	U[a] ppm	Pb[a*] ppm	$^{206}Pb^{a}/^{204}Pb$	Pb[c] pg	$^{208}Pb^{c}/^{206}Pb$	$^{207}Pb^{2}/^{235}U$	±1 SE	$^{206}Pb^{2}/^{238}U$	±1 SE	Corr. Coeff.	$^{207}Pb^{2}/^{206}Pb$	±1 SE	Apparent Age (Ma) $^{206}Pb/^{238}U$	+/-[3]	$^{207}Pb/^{235}U$	+/-[3]	$^{207}Pb/^{206}Pb$	+/-[3]	% Disc
GC01-146 Jimmy Hill Granite (Z7084; 45.4041°N 66.7146°E)																						
1	Z,Co,Clr,Eu,St,Abr,M1°	1	18	257.3	17.1	6552	3	0.16	0.4785	0.0007	0.063	0.00008	0.83900	0.05479	0.00005	396.0	0.9	397.1	1.0	403.5	3.8	1.9
2	Z,Co,Clr,El,Pr,Abr,M1°	1	11	179.8	13.9	2914	3	0.36	0.4787	0.001	0.063	0.00009	0.77000	0.05472	0.00007	396.5	1.1	397.2	1.4	400.8	5.9	1.1
3	Z,Co,Clr,St,Abr,Dia	25	23	503.4	34.3	4140	11	0.20	0.4783	0.0007	0.063	0.00008	0.89854	0.05478	0.00004	395.8	0.9	396.9	1.0	403.1	3.1	1.9
4	Z,Co,Alt,Pr,Abr,Dia	1	17	224.7	15.2	2164	4	0.18	0.4811	0.0012	0.064	0.00012	0.67853	0.05481	0.00010	397.8	1.5	398.8	1.6	404.5	8.1	1.7
5	Z,Co,Clr,Pr,Abr,Dia	27	18	350.0	24.7	5113	5	0.21	0.4959	0.0007	0.065	0.00007	0.83284	0.05541	0.00004	405.4	0.8	408.9	0.9	428.7	3.4	5.6
6	Z,Co,Clr,Pr,Abr,Dia	7	21	343.7	23.3	1366	22	0.16	0.498	0.0009	0.065	0.00007	0.76928	0.05581	0.00007	404.3	0.8	410.4	1.2	444.8	5.5	9.4
7	T,Br,Clr,Sub,Abr,M-0.5A	20	356	119.1	17.7	195.7	947	1.64	0.4779	0.0051	0.064	0.00019	0.68945	0.05434	0.00048	398.6	2.3	396.6	7.0	385.2	39.5	-3.6
8	T,Br,Clr,fFr,Sub,Abr,M-0.5A	18	289	110.3	16.6	181.8	771	1.67	0.478	0.0053	0.064	0.00020	0.69668	0.05443	0.00049	398.0	2.4	396.7	7.2	389	40.2	-2.4
Kedron-01 Kedron Granite (Z7531; 45.3066°N 67.1625°E)																						
9	M,pY,Alt,fFr,An,Fg,NAbr,M-0.5A	5	18	67.5	249.1	51.7	140	67.60	0.3738	0.0305	0.062	0.00069	0.61728	0.04375	0.00330	387.6	8.3	322.5	45.1	-124.6	335.7	-
10	M,pY,Alt,An,Fg,NAbr,M-0.5A	5	13	55.0	250.8	104.3	31	87.80	0.3711	0.0092	0.059	0.00034	0.61936	0.04549	0.00098	370.6	4.2	320.5	13.6	-29.5	101.6	-
11	M,Co,Clr,An,Fg,NAbr,M-0.5A	7	12	64.7	188.7	531.2	6	57.43	0.3595	0.0028	0.057	0.00018	0.51029	0.04537	0.00031	360.3	2.2	311.9	4.2	-35.9	32.7	-
12	Th,Y,Clr,Sub,NAbr,NM-0.5A	9	7	38313.0	289.3	21.2	13016	0.80	0.0504	0.0178	0.005	0.00025	0.71827	0.07850	0.02486	30.0	3.2	50.0	34.4	1159.6	914.2	97.6
02-SC-055 Tower Hill Microgranite Dyke (Z7530; 45.3066°N 67.1625°E)																						
13	Z,Co,Clr,Eu,Pr,Abr,Dia	47	12	196.5	14.5	1070	9	0.25	0.4985	0.0016	0.066	0.00012	0.60682	0.05507	0.00014	409.9	1.4	410.7	2.2	415.1	11.4	1.3
14	Z,Co,Clr,El,Eu,Pr,Abr,M1°	33	7	167.5	12.3	723.1	6	0.25	0.495	0.0022	0.065	0.00016	0.57608	0.05490	0.00020	408.3	1.9	408.3	3.0	408.1	16.1	-0.1
15	Z,Co,Alt,El,Eu,Pr,Abr,M1°	70	9	154.6	11.5	867.6	7	0.26	0.4936	0.0024	0.065	0.00014	0.52823	0.05476	0.00023	408.3	1.7	407.4	3.3	402.4	18.6	-1.5
GC01-163 Clarence Stream Granite Dyke (Z7302; UTM 19T, 0659655, 5024277)																						
16	M,Y,Clr,Eu,Pr,NAbr,M-0.5	1	17	1335.7	579.5	51146	1	6.84	0.4762	0.0006	0.063	0.00006	0.90888	0.05446	0.00003	396.4	0.7	395.5	0.8	390.2	2.2	-1.6
17	M,Y,Clr,Eu,Pr,NAbr,NM-0.5A	2	19	1591.0	647.8	22156	5	6.36	0.476	0.0006	0.063	0.00006	0.92096	0.05443	0.00003	396.4	0.7	395.3	0.8	388.7	2.2	-2.0
18	M,Co,Alt,Eu,Pr,NAbr,M-0.5A	2	9	1533.3	650.7	15020	4	6.67	0.4764	0.0006	0.063	0.00006	0.90888	0.05448	0.00003	396.4	0.8	395.6	0.8	390.8	2.3	-1.5

[1] Fractions are numbered sequentially through the entire manuscript
[2] Errors on atomic ratios are 1 standard error of mean; corrected for fractionation, spike and blank common Pb (At% 208:207:206 = 50.97:21.36:25.29)
[3] Error on $^{207}Pb/^{206}$ Pb age is 2 standard error in Ma
* Radiogenic Pb
a Includes sample weight error of 0.001 mg in concentration uncertainty;
b corrected for fractionation and spike only:
c Common Pb in analysis
** Fraction description abreviations:
Mineral type: Z, zircon; M, Monazite; T, titanite; Th, thorite
Colour: Co, colourless; pY, pale yellow; Y, yellow; Br, brown
Clarity: Clr, clear; Alt, altered; **Fractures**: fFr, few
Morphology: An, anhedral; Eu, euhedral; El, elongate; Fg, fragment; Pr, prismatic; St, stubby prism; Sub, subhedral; Tab, tabular,Ndl, needles
Abrasion: Abr, abraded; NAbr, not abraded
Magnetic properties: M-0.5A, magnetic at 0.5 Amps; M-0.75A, magnetic at 0.75 Amps; Dia, diamagnetic; NM0°, nonmagnetic at 0° side slope, NM1°, nonmagnetic at 1° side slope; M3°, magnetic at 3° side slope.
Corr. Coeff., correlation coefficient; %Disc., discordance in per cent

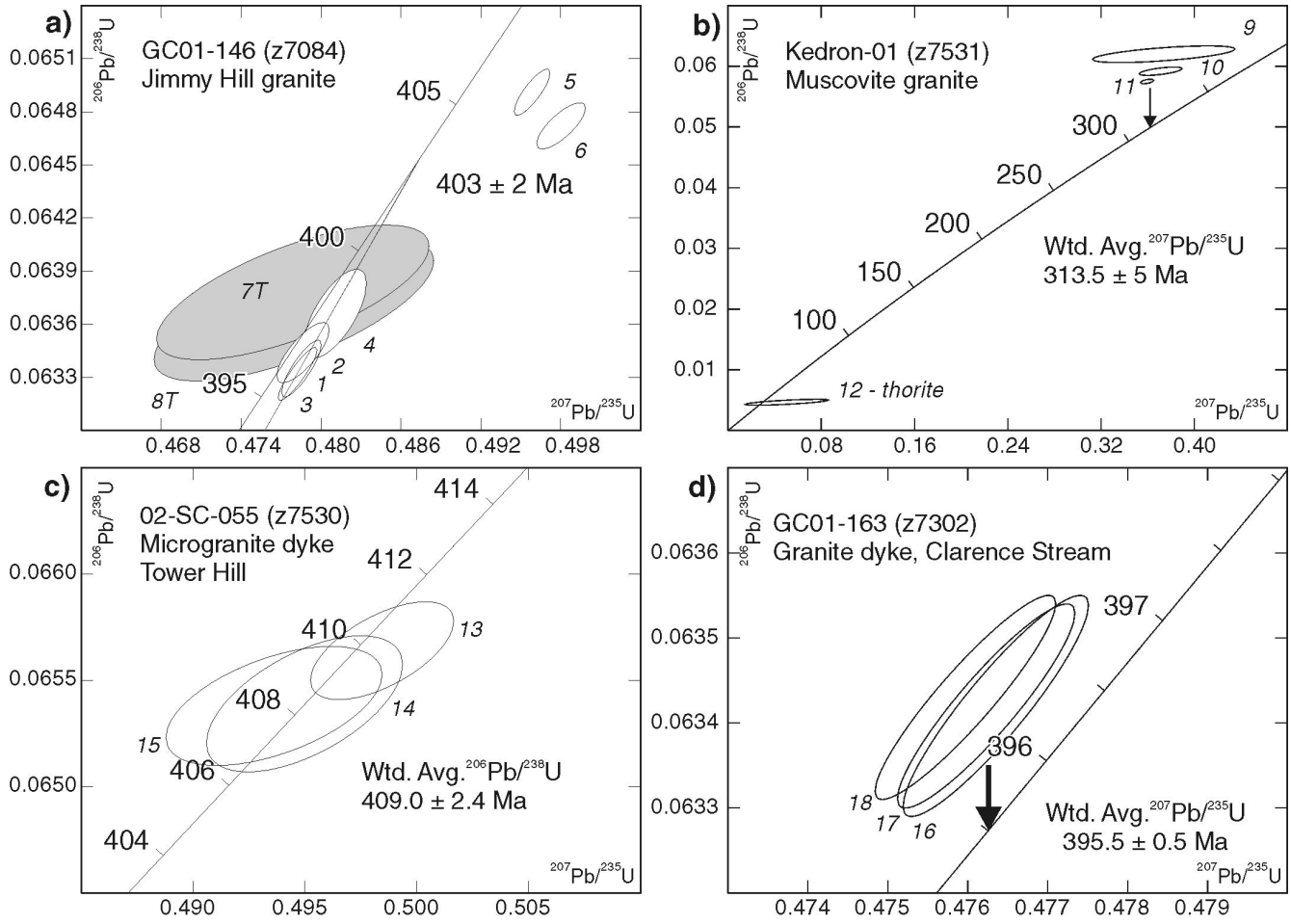

***Figure 2**. U-Pb concordia diagrams for samples analysed by TIMS method.*

Rb-Sr muscovite age of 401 ± 4 Ma for the main Tower Hill pluton, and provides a maximum age for the mineralization at Tower Hill.

Clarence Stream gold deposit

The main zone of the Clarence Stream gold deposit is located in the contact zone of Magaguadavic granite in Silurian volcano-sedimentary rocks of the Mascarene Belt (Waweig Formation; Fyffe and Thorne, 2002), southeast of the Sawyer Brook Fault (Locality 1, Fig. 1b, 3). The mineralization is controlled by heterogeneous, ductile-brittle dextral shear zones associated with the Sawyer Brook Fault, and is hosted by gabbroic bodies of the East Branch Brook intrusion and hornfelsed metasedimentary units of the Mascarene Group (Thorne et al., 2001, 2002a; Thorne and Lentz, 2001). These authors documented visible and nonvisible gold associated with arsenopyrite, pyrrhotite, stibnite, and a host of other metallic minerals disseminated in host rocks, in quartz veins, and locally in pegmatite veins. The mineralization is associated with silicification and sericitization, which predate an episode of epidote alteration. The spatial association with the Magaguadavic granite (the closest distance is less than 200 m), the presence of Au mineralization in pegmatite and aplitic dykes chemically similar to late phases of the Magaguadavic granite, the intimate relationship between pegmatite and the mineralized quartz veins, and the positive correlations of Au-Bi and Au-Sb suggest that the mineralization is genetically related to granitic intrusions (Thorne et al., 2001; Chi et al., 2001).

The auriferous quartz and pegmatite veins intrude foliated gabbros and metasedimentary rocks, and locally show extensional features such as angular fragments of wall rocks within the veins, but they also are commonly boudinaged, sheared and transposed to parallel with the shear zones. Z-folds produced by asymmetric deformation of quartz veins are compatible with dextral movement along the shear zones, which may be related to precursor structures of the Sawyer Brook Fault (Castonguay et al., 2003). Based on these relationships, dyke and vein emplacement (and indirectly gold mineralization) took place during and slightly after the development of the main foliation (S_3?), but before significant strain along the late shear zones.

Two samples were collected from the Clarence Stream area for U-Pb dating (Fig. 3) to constrain the age of gold mineralization. Sample GC01-150, taken from Trench 4 (Fig. 3a), is from a small auriferous pegmatite dyke (Fig. 4a) that is

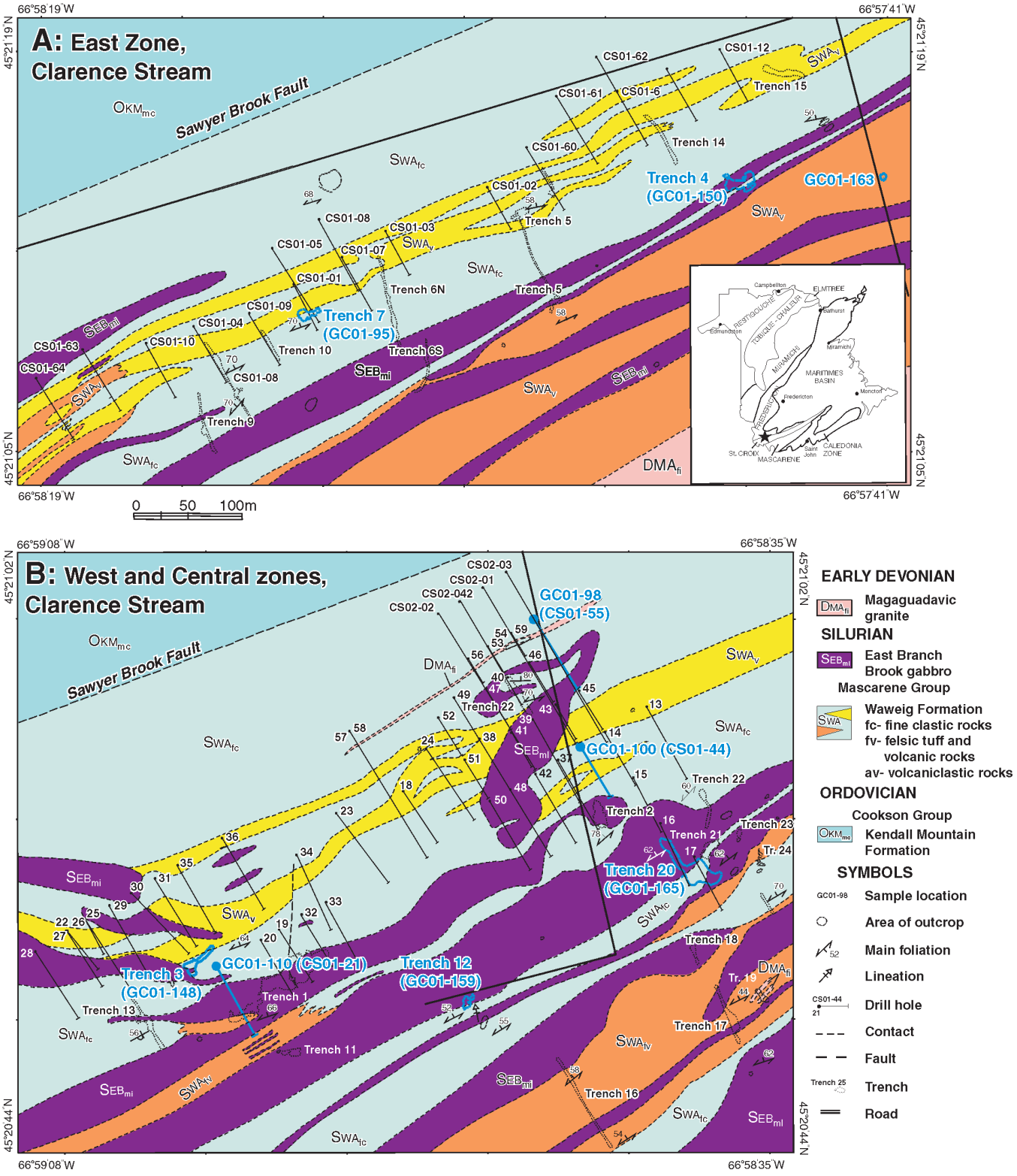

Figure 3. *Simplified geological map of the east zone* ***(a)*** *and west, central zones* ***(b)*** *of the main zone of the Clarence Stream gold deposit with geochronological sample locations (modified from Thorne et al., 2002b, c).*

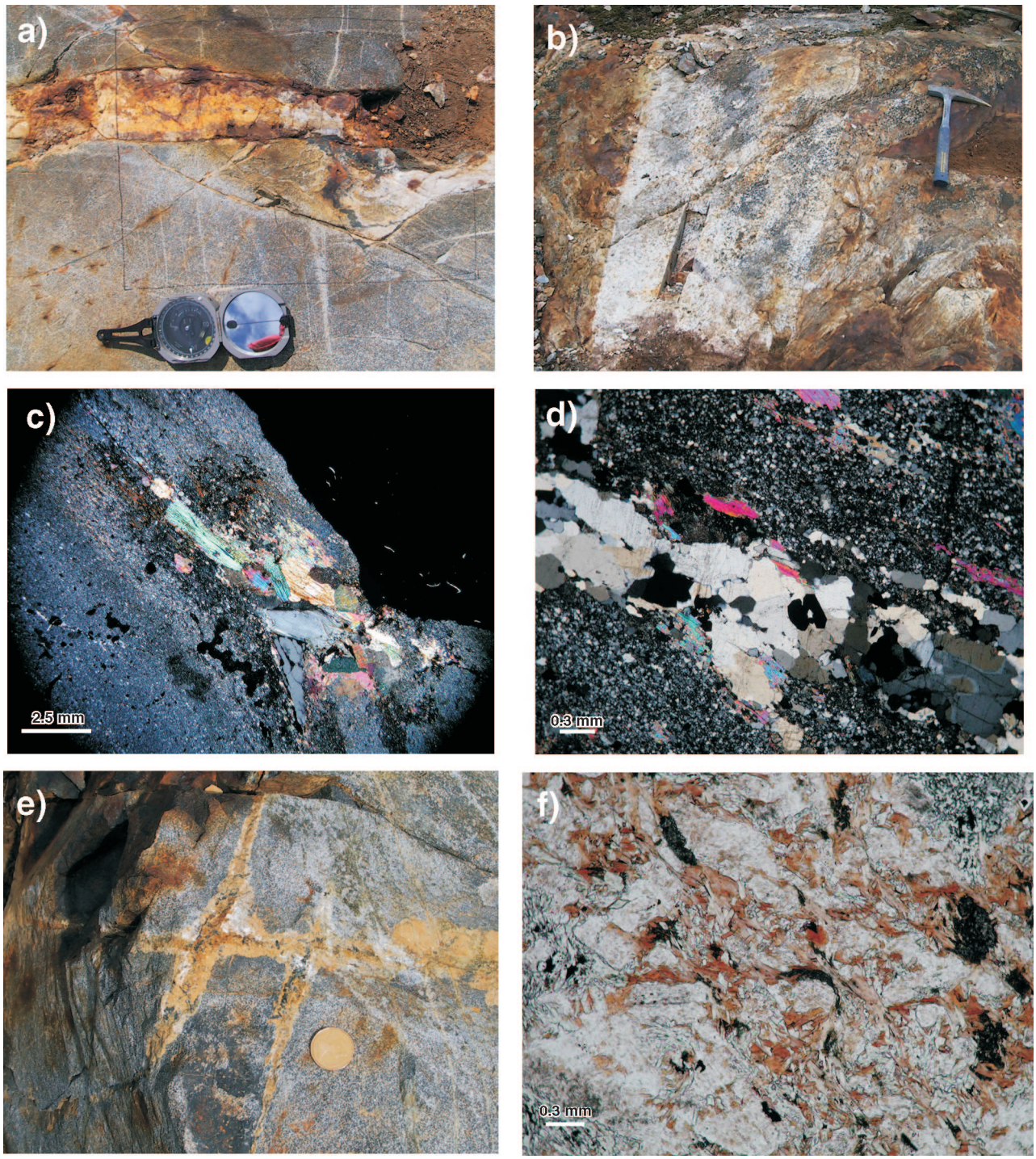

Figure 4. *Field and microphotographs.* ***a)*** *A boudinaged pegmatite-quartz vein containing sulphide and gold mineralization. Trench 4, east zone, Clarence Stream. Sample GC01-150 was collected from the dyke for U-Pb (zircon) dating.* ***b)*** *A weakly foliated granitic dyke intruding strongly foliated metasedimentary rocks. Outcrop near the roadside in the east zone, Clarence Stream. Sample GC01-163 was collected from the dyke for U-Pb (monazite) and $^{40}Ar/^{39}Ar$ (biotite) dating.* ***c)*** *GC01-148: A pod-like quartz-muscovite vein in hornfels, from an angular float in Trench 3, west zone, Clarence Stream. Muscovite was sampled for $^{40}Ar/^{39}Ar$ dating.* ***d)*** *GC01-95: a quartz-muscovite-sulphide veinlet in hornfels and muscovite along foliation planes, Trench 7, east zone, Clarence Stream. Muscovite was sampled for $^{40}Ar/^{39}Ar$ dating.* ***e)*** *GC01-159: Hornblende veins cutting gabbro, Trench 12, west zone, Clarence Stream. The hornblende in the vein was sampled for $^{40}Ar/^{39}Ar$ dating.* ***f)*** *GC01-100: hornfelsed gabbro containing abundant biotite resulting from thermal metamorphism, DDH CS01-44 (64.63–64.85m), central zone, Clarence Stream. Biotite was sampled for $^{40}Ar/^{39}Ar$ dating.*

transitional to a gold-bearing quartz vein. The dyke intrudes weakly foliated gabbro sheets interlayered with strongly deformed metasedimentary beds, and is boudinaged. A previous study of monazite from a pegmatite dyke in Trench 4 has yielded an electron microprobe chemical date of 390 ± 8 Ma, with an indication of older inherited monazite in the sample (Thorne et al., 2002a). Sample GC01-163 is from a granitoid dyke exposed on a roadside outcrop about 100 m east of Trench 4 (Fig. 3a). The dyke cuts foliated host rocks, and is weakly foliated (Fig. 4b). Quartz and feldspar are variably strained, as shown by undulatory extinction under a microscope. The relative timing of intrusion of the dyke to deformation fabrics is similar to that described above for the auriferous pegmatite dykes. Thus it provides a minimum age for early development of the foliation and a maximum age for the later strain that was responsible for the formation of boudins and asymmetric folding of the veins and dykes.

In addition to the U-Pb analyses, eight $^{40}Ar/^{39}Ar$ analyses were made for biotite, muscovite, and hornblende to assess the timing of regional metamorphism, dyke emplacement, and mineralization. Three muscovite-bearing samples were collected in the Clarence Stream area (Fig. 3) to provide minimum age estimates of mineralization. Sample GC01-165 is from a muscovite-bearing aplite dyke in Trench 20 (Fig. 3b), megascopically similar to the auriferous pegmatite dykes in Trench 4 (e.g. sample GC01-150). Sample GC01-148 is from a pod-like quartz vein that contains coarse muscovite and cuts the deformed metasedimentary units (Fig. 4c). The sample was collected from an angular float from Trench 3 in the west zone (Fig. 3b), and is interpreted to be from the adjacent mineralization zone. GC01-95 is from a muscovite-plated recrystallized quartz vein containing sulphide mineralization (Fig. 4d) that lies parallel with the main foliation in strongly foliated metasediments from Trench 7 in the east zone (Fig. 3a).

$^{40}Ar/^{39}Ar$ analyses on hornblende were carried out on three samples. Sample GC01-159 is from a hornblende vein within gabbro (Fig. 4e), collected from Trench 12 of the west zone (Fig. 3b). The vein and host rock at this locality are undeformed, but elsewhere similar veins cut a foliation, and are also folded. Samples GC01-98 and GC01-110 are relatively fresh gabbros taken from drill cores (Fig. 3b). The $^{40}Ar/^{39}Ar$ analysis of the hornblende from the gabbros is meant to provide a constraint on the cooling (500±50°C) ages of the gabbro intrusions or thermal metamorphism. GC01-159 is a thermally metamorphosed gabbro that contains abundant biotite (Fig. 4e). The $^{40}Ar/^{39}Ar$ age of the metamorphic biotite provides a constraint on the timing of thermal metamorphism and cooling (300±50°C).

U-Pb results

GC01-150 — boudinaged, mineralized pegmatite dyke (Trench 4; east zone)

Zircon grains recovered from the mineralized pegmatite dyke form a diverse population of morphological types with no clear magmatic component. No monazite was recovered. Owing to low zircon recovery and the diversity of zircon

Table 2. Ion microprobe U-Pb analytical data (SHRIMP)

Analyses	U (ppm)	Th (ppm)	Th/U	pb* (ppm)	$^{204}Pb/^{206}Pb$ (ppb)	$^{204}Pb/^{206}Pb$	±	f(206)^{204}	$^{208*}Pb/^{206*}Pb$	±	$^{207*}Pb/^{235}U$	±	$^{206*}Pb/^{238}U$	±	Corr Coeff	$^{207*}Pb/^{206*}Pb$	±	$^{206*}Pb/^{238}U$	±	$^{207*}Pb/^{206*}Pb$	±	Conc. (%)
GC01-150 Clarence Stream Pegmatite (Z7085; 45.3558°N 66.9634°E)																						
7085-10.1	488.94	29.73	0.06282	28	2	0.00007	0.00009	0.00116	0.0189	0.0037	0.4650	0.0166	0.06239	0.00087	0.5008	0.0541	0.0017	390	5	373	72	104.5
7085-10.2	638.07	49.01	0.07935	38	0	0.00001	0.00001	0.00017	0.0248	0.0018	0.4958	0.0134	0.06459	0.00080	0.5656	0.0557	0.0013	403	5	439	51	91.9
7085-11.1	334.86	231.33	0.71366	23	9	0.00050	0.00017	0.00864	0.2225	0.0131	0.4711	0.0261	0.06327	0.00079	0.3434	0.0540	0.0028	395	5	371	123	106.6
7085-6.1	342.62	103.05	0.31073	22	1	0.00005	0.00007	0.00078	0.1070	0.0073	0.4878	0.0145	0.06335	0.00096	0.6104	0.0558	0.0013	396	6	446	54	88.8
7085-3.1	224.79	16.02	0.07364	13	1	0.00009	0.00016	0.00152	0.0273	0.0065	0.4894	0.0247	0.06337	0.00083	0.3766	0.0560	0.0026	396	5	453	108	87.5
7085-9.1	122.88	45.83	0.3853	8	2	0.00036	0.00028	0.00629	0.1007	0.0132	0.4351	0.0417	0.06398	0.00106	0.2931	0.0493	0.0046	400	6	163	203	245.2
7085-8.1	126.37	81.64	0.66739	9	2	0.00022	0.00021	0.00385	0.2256	0.0141	0.4628	0.0332	0.06433	0.00098	0.3311	0.0522	0.0036	402	6	293	164	137.1
7085-1.1	453.74	121.84	0.27741	29	0	0.00001	0.00005	0.00015	0.0859	0.0050	0.4822	0.0132	0.06471	0.00091	0.6130	0.0541	0.0012	404	6	373	50	108.3
7085-5.1	572.07	389.19	0.7028	41	1	0.00003	0.00004	0.00053	0.2182	0.0065	0.5039	0.0110	0.06545	0.00076	0.6315	0.0558	0.0010	409	5	446	38	91.6
7085-7.1	167.07	75.82	0.46883	42	0	0.00000	0.00006	0.00006	0.1486	0.0061	2.7985	0.0703	0.23448	0.00297	0.6049	0.0866	0.0018	1358	16	1351	39	100.5
7085-2.1	119.82	64.99	0.56037	52	0	0.00001	0.00001	0.00017	0.1621	0.0040	7.0654	0.1128	0.38965	0.00523	0.8973	0.1315	0.0009	2121	24	2118	13	100.1

Notes (see Stern, 1997; Stern and Amelin, 2003 for analytical details):
Analyses: sample number-grain number analysis number. Ion probe mount number IP240
Uncertainties reported at 1σ (absolute) and are calculated by numerical propagation of all known sources of error
Calibration standard : BR266 - Age 559.0 Ma; $^{206}Pb/^{238}U = 0.09059$; error 1.0%
f206^{204} refers to mole fraction of total ^{206}Pb that is due to common Pb, calculated using the ^{204}Pb-method; common Pb composition used is the surface blank: 4/6: 0.05770; 7/6: 0.89500; 8/6: 2.13840
Discordance relative to origin = 100 * (1-($^{206}Pb/^{238}U$ age)/($^{207}Pb/^{206}Pb$ age))

morphological types that is indicative of a dominantly inherited population, a subset of zircon grains was analyzed by the SHRIMP method (Table 2). Individual grains range in composition from 120 to 650 ppm U, with variable Th/U ratios of 0.07 to 0.71. With the exception of two grains that have Proterozoic dates (2118 Ma, 1350 Ma), the majority of grains have $^{206}Pb/^{238}U$ ages of ca. 400 Ma. Statistically, the nine analyses define a single age population at 400 ± 5 Ma (MSWD = 1.3; Fig. 5). However, since they are likely inherited grains, the age must be considered a maximum for the intrusion of the pegmatite. As these grains are significantly younger than the depositional age of the Mascarene Group (Miller and Fyffe, 2002), they are most likely derived from igneous precursors of the Magaguadavic granite. This result is consistent with the 390 ± 8 Ma chemical age of monazite determined by Thorne et al. (2002a). The significantly older Proterozoic zircons are presumably derived from sedimentary rocks within the area.

GC01-163 — deformed, late-foliation granitoid dyke (roadside near Trench 4; east zone)

Monazite grains recovered from this sample yield reproducible, reversely discordant ages (Table 1; Fig. 2d). The reverse discordance is attributed to initial disequilibrium (Scharer, 1984), and the weighted mean $^{207}Pb/^{235}U$ age of 395.5 ± 0.5 Ma (MSWD = 0.15) is taken as the crystallization age of the intrusion. This represents a minimum age for the development of the foliation in the country rock.

$^{40}Ar/^{39}Ar$ Results

Results of $^{40}Ar/^{39}Ar$ analyses are illustrated in Figure 6 and data presented in Table 3. Age interpretations are based on plateau age spectrum, as there is no evidence for excess argon in the minerals sampled (Appendix 1).

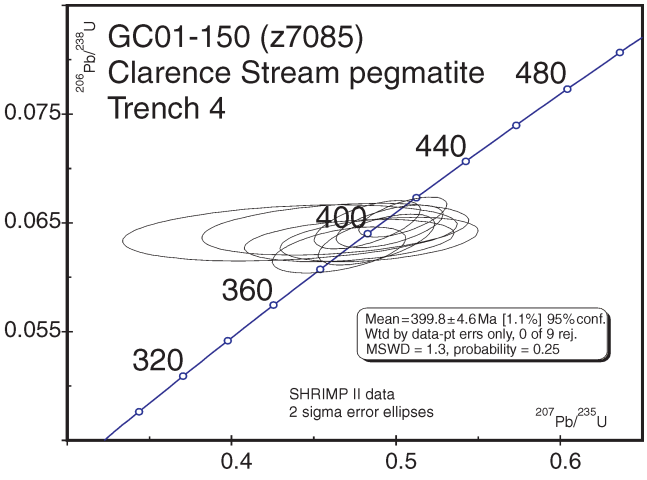

Figure 5. *U-Pb Concordia diagram of zircon analysed by SHRIMP method from sample GC01-150. Two zircon grains with Paleoproterozoic dates are not shown (see Table 2). Ellipses shown at 95% confidence level.*

GCC01-163

Sample GC01-163, described above, has a monazite crystallization age of 395.5 ± 0.5 Ma. $^{40}Ar/^{39}Ar$ analyses of biotite from the sample did not yield an interpretable age spectrum (Fig. 6a). Analyses of two separate aliquots produced a humped age spectrum indicating disturbance of the Ar system in this sample, and no age is interpreted.

GC01-165

Analyses were made on muscovite from an aplite dyke in Trench 20. The Ar spectrum for this sample is characterized by a flat plateau with no significant evidence for disturbance, and a plateau age of 395.6 ± 3.6 Ma (Fig. 6b). The first step contained a small proportion of gas, had an older apparent age, and was excluded from the age calculation. This age is within error of age of the granite dyke GC01-163.

GC01-148

Muscovite from the quartz vein in the Trench 3 area yielded an 11-step Ar spectrum with a well defined plateau age of 388.8 ± 3.6 Ma (Fig. 6c).

GC01-95

Muscovite from the sulphide-bearing quartz vein from Trench 7 yielded a ten-step plateau age of 389.3 ± 3.5 Ma (Fig. 6d).

GC01-100

Replicate analyses of biotite from GC01-100 yielded reproducible age spectra with a combined plateau age of 390.9 ± 3.6 Ma. Biotite in this sample is of metamorphic origin and the age represents cooling (at 300°C) following thermal metamorphism. The sample shows evidence for some disturbance of the Ar system in the lower wattage steps. These were excluded from the age calculation (Fig. 6e)

GC01-159

Analyses of hornblende from the vein in gabbro, sample GC01-159, yielded an imprecise plateau age of 397 ± 26 Ma, based on analyses of two aliquots (Fig. 6f).

GC01-110

Two replicate analyses of hornblende in this sample of relatively fresh gabbro in drill core yielded a combined plateau age of 393.8 ± 18 Ma (Fig. 6g).

Table 3. Ar-Ar analytical data

Power[a]	Volume ^{39}A x10^{-11} cc	^{36}Ar/^{39}Ar	^{37}Ar/^{39}Ar	^{38}Ar/^{39}Ar	^{40}Ar/^{39}Ar	%^{40}Ar atmospheric	*^{40}Ar/^{39}Ar	f_{39}[b] (%)	Apparent Age Ma[c]
GC01-163 Biotite; J=.02364430 (Z7302; UTM: 19T 0659655 - 5024277)									
Aliquot: A									
2.4	14.159	0.0118±0.0004	0.021±0.001	0.074±0.011	10.217±0.037	34.1	6.731±0.121	2.4	266.44±4.45
2.8	22.4575	0.0008±0.0001	0.010±0.001	0.077±0.011	9.617±0.035	2.3	9.393±0.041	3.7	361.82±1.44
3	64.2757	0.0002±0.0000	0.004±0.000	0.082±0.011	10.384±0.037	0.5	10.337±0.038	10.7	394.47±1.29
3.3	23.6958	0.0001±0.0001	0.006±0.001	0.087±0.011	10.396±0.039	0.3	10.365±0.045	3.9	395.44±1.55
3.5	29.0241	0.0001±0.0001	0.007±0.001	0.085±0.011	10.454±0.038	0.2	10.438±0.042	4.8	397.92±1.43
3.9	38.7107	0.0001±0.0001	0.006±0.000	0.082±0.011	10.572±0.033	0.1	10.560±0.037	6.4	402.12±1.25
4.2	26.9888	0.0001±0.0001	0.008±0.001	0.083±0.011	10.655±0.042	0.2	10.629±0.049	4.5	404.46±1.67
4.6	19.0344	0.0002±0.0001	0.008±0.001	0.084±0.011	10.612±0.042	0.4	10.573±0.051	3.2	402.55±1.76
5	10.0943	0.0002±0.0002	0.017±0.001	0.087±0.011	10.647±0.040	0.6	10.588±0.067	1.7	403.08±2.29
6	7.9801	0.0004±0.0003	0.027±0.002	0.087±0.011	10.599±0.061	1	10.490±0.083	1.3	399.71±2.83
12	30.0674	0.0001±0.0001	0.010±0.000	0.088±0.011	10.481±0.038	0.2	10.455±0.047	5	398.53±1.62
Aliquot: B									
2.8	87.7642	0.0013±0.0000	0.005±0.001	0.102±0.011	9.807±0.034	4	9.417±0.034	14.6	362.65±1.19
3	87.7249	0.0001±0.0000	0.004±0.000	0.104±0.011	10.402±0.016	0.1	10.388±0.018	14.6	396.22±0.60
3.3	18.1574	0.0001±0.0001	0.013±0.001	0.107±0.011	10.389±0.021	0.1	10.381±0.039	3	396.00±1.32
3.5	25.0731	0.0000±0.0001	0.010±0.001	0.108±0.011	10.469±0.024	0	10.468±0.033	4.2	398.96±1.14
3.9	25.6437	0.0000±0.0001	0.010±0.001	0.108±0.011	10.580±0.022	0	10.578±0.030	4.3	402.73±1.04
4.2	16.6297	0.0001±0.0001	0.017±0.001	0.110±0.011	10.645±0.035	0.1	10.634±0.048	2.8	404.63±1.62
4.6	10.8487	0.0002±0.0002	0.027±0.002	0.109±0.011	10.685±0.040	0.5	10.634±0.068	1.8	404.64±2.32
6	13.5357	0.0001±0.0002	0.022±0.001	0.110±0.011	10.569±0.033	0.1	10.554±0.052	2.2	401.89±1.76
12	31.2607	0.0000±0.0001	0.007±0.001	0.105±0.011	10.551±0.028	0.1	10.545±0.037	5.2	401.59±1.27
GC01-165 Muscovite; J=.02369050 (Z7186; UTM: 19T 0658540 - 5023384)									
Aliquot: A									
2.4	5.248	0.0108±0.0006	0.006±0.008	0.009±0.011	13.668±0.074	23.3	10.478±0.148	0.8	400.01±5.08
2.8	47.9905	0.0003±0.0001	0.000±0.001	0.003±0.011	10.427±0.022	0.8	10.340±0.025	7.1	395.27±0.86
3	86.7155	0.0001±0.0000	0.000±0.001	0.002±0.011	10.387±0.021	0.4	10.347±0.023	12.9	395.53±0.80
3.3	9.7424	0.0001±0.0003	0.001±0.003	0.003±0.011	10.409±0.110	0.3	10.377±0.128	1.5	396.56±4.39
3.5	256.7622	0.0001±0.0000	0.002±0.000	0.003±0.011	10.402±0.034	0.4	10.362±0.036	38.2	396.04±1.22
3.7	18.2568	0.0000±0.0001	0.000±0.002	0.003±0.011	10.394±0.055	0	10.390±0.061	2.7	396.98±2.10
3.9	19.3981	0.0001±0.0002	0.001±0.002	0.003±0.011	10.350±0.046	0.1	10.338±0.064	2.9	395.20±2.20
4.2	17.3658	0.0001±0.0002	0.001±0.002	0.003±0.011	10.359±0.036	0.1	10.348±0.048	2.6	395.56±1.65
4.6	14.7654	0.0000±0.0002	0.001±0.003	0.003±0.011	10.339±0.032	0.1	10.331±0.053	2.2	394.96±1.82
5.5	9.2433	0.0001±0.0003	0.001±0.005	0.004±0.011	10.250±0.064	0.3	10.223±0.094	1.4	391.24±3.25
12	186.7122	0.0001±0.0000	0.003±0.001	0.003±0.011	10.389±0.043	0.3	10.353±0.045	27.8	395.72±1.55
GC01-148 Muscovite; J=.02351710 (Z7187; UTM: 19T 0657975 - 5023519)									
Aliquot: A									
2.4	4.3692	0.0012±0.0006	0.036±0.003	0.003±0.011	10.614±0.071	2.3	10.372±0.182	3.6	393.75±6.20
2.8	51.7745	0.0001±0.0000	0.004±0.000	0.002±0.011	10.230±0.032	0.1	10.216±0.034	42.3	388.46±1.15
3	22.2589	0.0001±0.0001	0.008±0.001	0.003±0.011	10.236±0.036	0.1	10.228±0.048	18.2	388.86±1.66
3.3	3.2406	0.0003±0.0008	0.046±0.003	0.004±0.011	10.234±0.076	0.5	10.185±0.195	2.7	387.38±6.67
3.5	3.7867	0.0003±0.0006	0.042±0.005	0.004±0.011	10.247±0.078	0.3	10.214±0.154	3.1	388.36±5.26
3.9	2.1443	0.0007±0.0012	0.068±0.005	0.008±0.011	10.239±0.147	0	10.243±0.350	1.8	389.36±11.95
4.2	3.5179	0.0002±0.0007	0.038±0.006	0.004±0.011	10.231±0.105	0.3	10.204±0.179	2.9	388.03±6.13
4.6	1.1766	0.0003±0.0023	0.126±0.013	0.011±0.011	10.294±0.210	0.8	10.211±0.526	1	388.27±18.01
5	3.3055	0.0005±0.0007	0.034±0.010	0.005±0.011	10.233±0.089	0.2	10.211±0.201	2.7	388.27±6.87
6	6.8058	0.0001±0.0004	0.024±0.002	0.004±0.011	10.243±0.059	0.2	10.227±0.098	5.6	388.81±3.37
12	19.9906	0.0000±0.0001	0.008±0.001	0.003±0.011	10.235±0.049	0.1	10.228±0.059	16.3	388.84±2.01

[a]: As measured by laser in % of full nominal power (10W)
[b]: Fraction ^{39}Ar as percent of total run
[c]: Errors are analytical only and do not reflect error in irradiation parameter J
[d]: Nominal J, referenced to FCT-SAN=28.03 Ma (Renne et al., 1994)
All uncertainties quoted at 2σ level

Table 3. (Cont.)

Power[a]	Volume ^{39}A x10^{-11} cc	^{36}Ar/^{39}Ar	^{37}Ar/^{39}Ar	^{38}Ar/^{39}Ar	^{40}Ar/^{39}Ar	%^{40}Ar atmospheric	*^{40}Ar/^{39}Ar	f_{39}[b] (%)	Apparent Age Ma[c]
GC01-95 Muscovite; J=.02354020 (Z7308; UTM: 19T 0659121 - 5024135)									
Aliquot: A									
2.4	1.2846	0.0064±0.0018	0.122±0.014	0.028±0.011	10.046±0.197	18	8.235±0.418	0.6	319.65±14.87
2.8	62.9942	0.0001±0.0000	0.003±0.000	0.002±0.011	10.266±0.021	0.3	10.235±0.023	29.1	389.45±0.79
3	71.8026	0.0000±0.0000	0.003±0.000	0.002±0.011	10.212±0.021	0.1	10.201±0.023	33.2	388.27±0.78
3.3	8.9135	0.0000±0.0003	0.022±0.006	0.003±0.011	10.236±0.037	0.1	10.222±0.059	4.1	388.98±2.02
3.5	23.8577	0.0001±0.0001	0.008±0.000	0.002±0.011	10.252±0.022	0.1	10.241±0.033	11	389.64±1.12
3.9	8.7312	0.0001±0.0003	0.023±0.005	0.003±0.011	10.281±0.043	0.2	10.261±0.070	4	390.32±2.39
4.2	10.5085	0.0001±0.0002	0.020±0.004	0.003±0.011	10.255±0.032	0.1	10.245±0.055	4.9	389.79±1.87
4.6	6.3068	0.0000±0.0005	0.026±0.002	0.003±0.011	10.301±0.052	0.1	10.291±0.078	2.9	391.35±2.66
5	9.8954	0.0002±0.0002	0.016±0.002	0.002±0.011	10.315±0.040	0.4	10.271±0.062	4.6	390.68±2.14
6	3.657	0.0001±0.0006	0.047±0.003	0.004±0.011	10.289±0.074	0.2	10.265±0.169	1.7	390.46±5.79
12	8.2882	0.0003±0.0003	0.023±0.001	0.002±0.011	10.339±0.048	0.6	10.277±0.079	3.8	390.87±2.71
GC01-100 Biotite; J=.02369630 (Z7307; DDH-44, 64.63-64.85 m)									
Aliquot: A									
2.4	4.8889	0.0032±0.0002	0.289±0.007	0.029±0.001	7.736±0.054	12.2	6.790±0.082	0.5	269.17±3.01
2.8	17.5643	0.0006±0.0001	0.263±0.005	0.025±0.011	8.476±0.033	2	8.308±0.040	1.7	324.20±1.44
3	40.0846	0.0002±0.0001	0.251±0.007	0.027±0.011	9.891±0.027	0.4	9.848±0.034	3.9	378.38±1.20
3.5	34.1324	0.0001±0.0001	0.298±0.007	0.029±0.011	10.055±0.039	0.2	10.037±0.045	3.3	384.91±1.55
3.9	68.637	0.0001±0.0000	0.416±0.009	0.029±0.011	10.028±0.035	0.3	10.001±0.042	6.6	383.68±1.45
4.2	52.5168	0.0001±0.0001	0.591±0.012	0.029±0.011	10.030±0.031	0.1	10.015±0.045	5.1	384.17±1.57
4.6	86.6576	0.0000±0.0000	0.469±0.009	0.030±0.011	10.086±0.011	0.1	10.078±0.027	8.3	386.36±0.92
5	37.3429	0.0000±0.0000	0.476±0.009	0.030±0.011	10.122±0.019	-0.2	10.142±0.034	3.6	388.56±1.17
6	228.3729	0.0001±0.0000	0.390±0.008	0.030±0.011	10.221±0.017	0.3	10.192±0.027	21.9	390.29±0.94
12	90.4002	0.0000±0.0000	0.772±0.014	0.033±0.011	10.207±0.035	0.1	10.198±0.052	8.7	390.48±1.81
Aliquot: B									
2.4	3.447	0.0031±0.0008	0.566±0.034	0.038±0.011	6.739±0.070	13.3	5.841±0.134	0.3	233.87±5.04
2.8	10.7908	0.0006±0.0003	0.394±0.012	0.031±0.011	3.950±0.024	4.6	3.770±0.049	1	154.36±1.93
3	13.5069	0.0005±0.0002	0.385±0.012	0.027±0.011	8.494±0.057	1.7	8.347±0.065	1.3	325.61±2.32
3.5	36.5976	0.0002±0.0001	0.483±0.014	0.030±0.011	9.837±0.043	0.5	9.786±0.051	3.5	376.23±1.78
3.9	21.5924	0.0000±0.0001	0.645±0.013	0.030±0.011	10.103±0.021	0.1	10.095±0.044	2.1	386.94±1.51
4.2	29.4488	0.0001±0.0001	0.835±0.017	0.030±0.011	10.177±0.020	0.4	10.136±0.049	2.8	388.36±1.68
4.6	49.2939	0.0001±0.0001	0.950±0.020	0.031±0.011	10.237±0.017	0.3	10.210±0.052	4.7	390.90±1.77
5	27.0664	0.0002±0.0001	0.785±0.016	0.031±0.011	10.302±0.031	0.5	10.252±0.053	2.6	392.34±1.81
5.5	63.8699	0.0001±0.0001	0.843±0.017	0.032±0.011	10.287±0.024	0.3	10.253±0.049	6.1	392.37±1.70
6	46.9598	0.0001±0.0001	0.581±0.013	0.030±0.011	10.306±0.024	0.3	10.279±0.039	4.5	393.26±1.34
12	77.5628	0.0001±0.0000	1.390±0.025	0.031±0.011	10.201±0.013	0.2	10.184±0.070	7.5	390.00±2.43
GC01-159 Hornblende; J=.02359800 (Z7306; UTM: 19T 0658213 - 5023455)									
Aliquot: A									
2.4	0.0131	0.5445±0.0983	48.639±46.332	4.414±4.202	588.123±559.825	82.3	104.100±109.918	0.1	2237.57±1492.48
2.8	0.006	0.1663±0.0811	62.306±119.992	2.455±4.731	227.920±439.695	98.2	4.194±105.251	0	170.25±10724.20
3	0.0008	0.0977±0.1004	489.408±7158.138	4.822±70.562	653.028±9553.597	94.6	35.121±985.691	0	1089.03±8678.08
3.5	2.1764	0.0195±0.0014	35.284±0.636	1.082±0.015	17.076±0.171	33.3	11.391±1.782	8.2	429.51±59.80
3.9	8.4647	0.0039±0.0005	29.002±0.446	0.988±0.012	11.511±0.074	9.7	10.392±1.443	31.9	395.68±49.33
4.2	0.753	0.0024±0.0037	32.066±0.792	0.927±0.026	10.513±0.313	2.9	10.211±1.844	2.8	389.46±63.28
4.6	0.9692	0.0035±0.0027	31.889±0.821	0.943±0.027	10.760±0.267	6.7	10.038±1.708	3.7	383.51±58.79
5	0.3702	0.0069±0.0066	30.981±1.401	0.924±0.040	10.700±0.559	12	9.414±2.236	1.4	361.91±77.91
6	0.5586	0.0050±0.0047	32.505±1.000	0.945±0.032	11.079±0.411	8.6	10.128±1.993	2.1	386.62±68.49
12	0.905	0.0041±0.0029	32.952±0.755	0.930±0.023	10.937±0.270	8	10.057±1.778	3.4	384.18±61.18

[a]: As measured by laser in % of full nominal power (10W)
[b]: Fraction ^{39}Ar as percent of total run
[c]: Errors are analytical only and do not reflect error in irradiation parameter J
[d]: Nominal J, referenced to FCT-SAN=28.03 Ma (Renne et al., 1994)
All uncertainties quoted at 2σ level

Table 3. (Cont.)

Power[a]	Volume ^{39}A x10^{-11} cc	^{36}Ar/^{39}Ar	^{37}Ar/^{39}Ar	^{38}Ar/^{39}Ar	^{40}Ar/^{39}Ar	%^{40}Ar atmospheric	*^{40}Ar/^{39}Ar	f_{39}[b] (%)	Apparent Age Ma[c]
Aliquot: B									
3	0.009	0.3243±0.1214	92.969±87.066	5.788±5.417	379.163±354.922	68.6	119.126±139.197	0	2413.75±1674.52
3.5	0.2045	0.0153±0.0116	44.800±3.181	1.168±0.090	14.070±1.215	24.9	10.571±3.799	0.8	401.76±129.49
3.9	1.255	0.0037±0.0021	30.676±0.719	1.161±0.022	11.172±0.208	7.6	10.322±1.606	4.7	393.28±54.98
5	9.3957	0.0006±0.0003	26.966±0.470	1.245±0.012	10.675±0.067	1.5	10.511±1.339	35.4	399.72±45.68
12	1.486	0.0019±0.0018	32.526±0.806	1.255±0.027	10.630±0.213	3.5	10.263±1.679	5.6	391.24±57.56
GC01-110 Hornblende; J=.02311940 (Z7305; DDH-21, 68.25-68.50 m)									
Aliquot: A									
2.8	0.02	1.4713±0.1386	76.098±45.699	5.039±3.021	1396.101±834.588	74.6	354.769±218.020	0.1	4004.10±1026.49
3	0.0707	0.3854±0.0379	19.103±3.598	0.502±0.094	167.865±30.677	93.4	11.075±10.185	0.3	411.26±338.93
3.5	0.1201	0.1901±0.0177	24.904±2.799	0.712±0.080	79.136±8.646	85.7	11.333±4.490	0.5	419.82±148.46
3.9	1.1657	0.0325±0.0024	36.169±0.930	1.143±0.029	23.363±0.462	41.4	13.684±1.908	5.1	495.89±60.46
4.2	2.4952	0.0062±0.0012	29.691±0.574	1.096±0.017	12.506±0.144	14.3	10.723±1.506	10.9	399.55±50.35
4.6	3.4998	0.0029±0.0007	26.277±0.512	1.096±0.017	11.461±0.136	7.2	10.641±1.316	15.3	396.81±44.06
5	2.303	0.0023±0.0010	25.736±0.463	1.084±0.015	10.818±0.115	5.6	10.215±1.295	10.1	382.50±43.71
6	0.7	0.0057±0.0030	29.911±0.791	1.056±0.025	11.374±0.300	12.9	9.903±1.635	3.1	371.94±55.49
12	1.7154	0.0040±0.0013	32.408±0.592	1.063±0.018	11.667±0.157	9.4	10.575±1.634	7.5	394.60±54.78
Aliquot: B									
4.2	1.9309	0.0421±0.0018	28.473±0.684	1.097±0.018	23.295±0.314	54	10.708±1.485	8.4	399.05±49.64
3	0.063	1.0060±0.0989	49.826±14.160	1.939±0.547	524.562±147.550	90	52.561±20.865	0.3	1434.86±395.09
4.6	5.3439	0.0038±0.0007	26.887±0.526	1.101±0.014	11.636±0.088	9.5	10.531±1.346	23.4	393.11±45.17
6	2.2301	0.0170±0.0014	27.814±0.581	1.158±0.019	15.684±0.200	32.2	10.629±1.437	9.8	396.40±48.11
12	1.2115	0.0042±0.0016	30.420±0.788	1.087±0.027	11.773±0.239	9.8	10.621±1.559	5.3	396.12±52.20
GC01-98 Amphibole; J=.02313670 (Z7304; DDH-55, 172.01-172.21 m)									
Aliquot: A									
3	0.1813	0.2830±0.0187	6.156±0.500	0.280±0.024	106.237±7.159	89.6	11.087±4.714	2.1	411.96±156.68
3.5	0.2114	0.2007±0.0132	6.167±0.444	0.202±0.018	81.117±5.085	81.6	14.961±2.689	2.4	536.24±83.38
4.2	0.917	0.0655±0.0035	24.885±0.609	0.305±0.017	29.552±0.458	66.9	9.772±1.485	10.5	367.74±50.57
4.6	1.4265	0.0325±0.0018	49.131±1.031	0.543±0.015	21.466±0.269	45.3	11.745±2.457	16.4	433.67±80.67
5.5	4.0579	0.0206±0.0009	52.129±0.944	0.541±0.012	16.970±0.143	36	10.853±2.593	46.5	404.16±86.52
12	1.9307	0.0036±0.0013	35.984±0.805	0.302±0.012	9.980±0.152	10.4	8.945±1.802	22.1	339.34±62.33

[a]: As measured by laser in % of full nominal power (10W)
[b]: Fraction ^{39}Ar as percent of total run
[c]: Errors are analytical only and do not reflect error in irradiation parameter J
[d]: Nominal J, referenced to FCT-SAN=28.03 Ma (Renne et al., 1994)
All uncertainties quoted at 2σ level

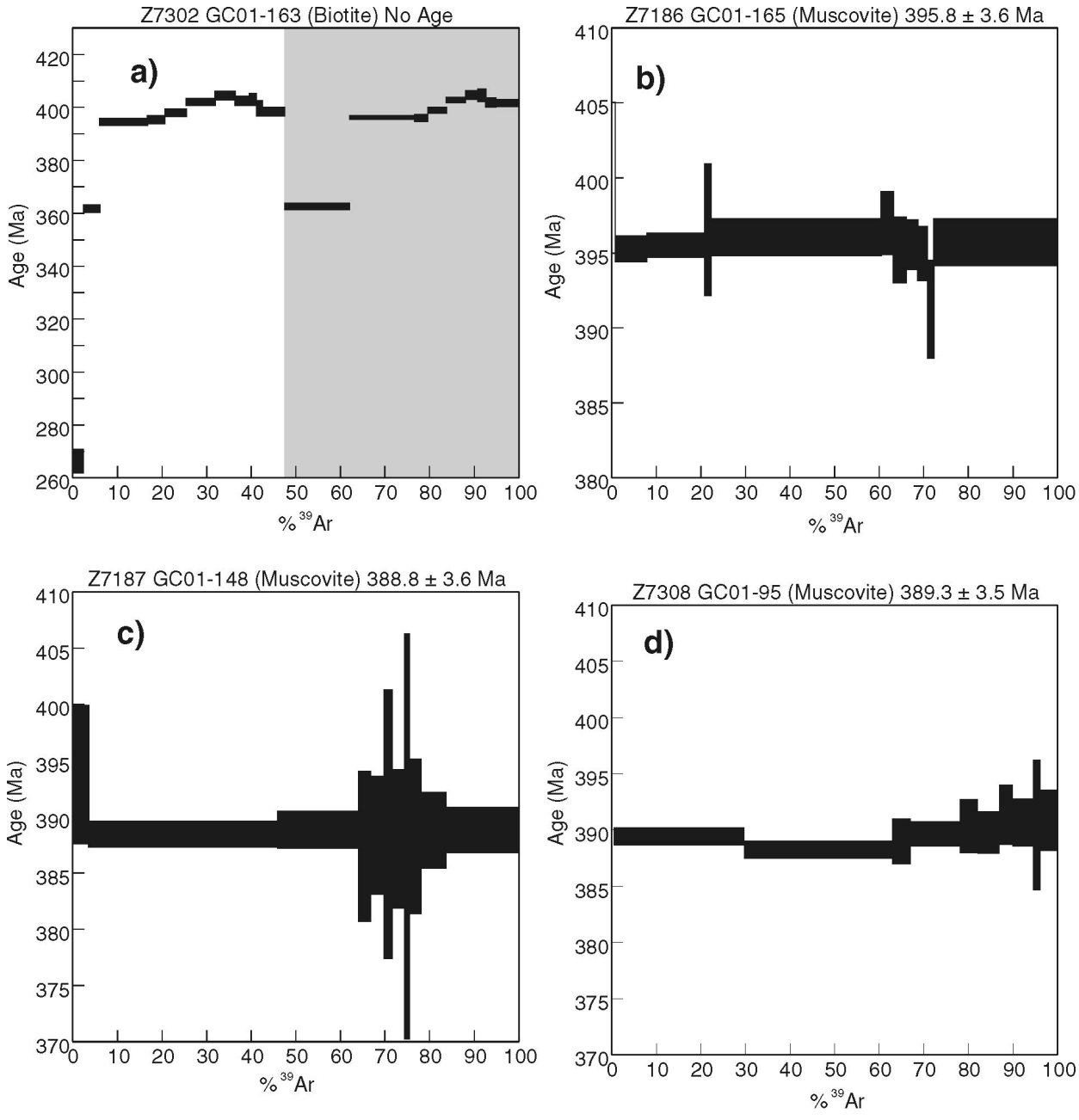

Figure 6. *Plots of step-heating, laser Ar-Ar gas-release spectrum. Plots a, e, f, and g include step-heating data from two or more aliquots, alternately shaded and normalized to the total volume of ^{39}Ar released. Upper part of e, f, g, and h plots Ca/K ratio.*

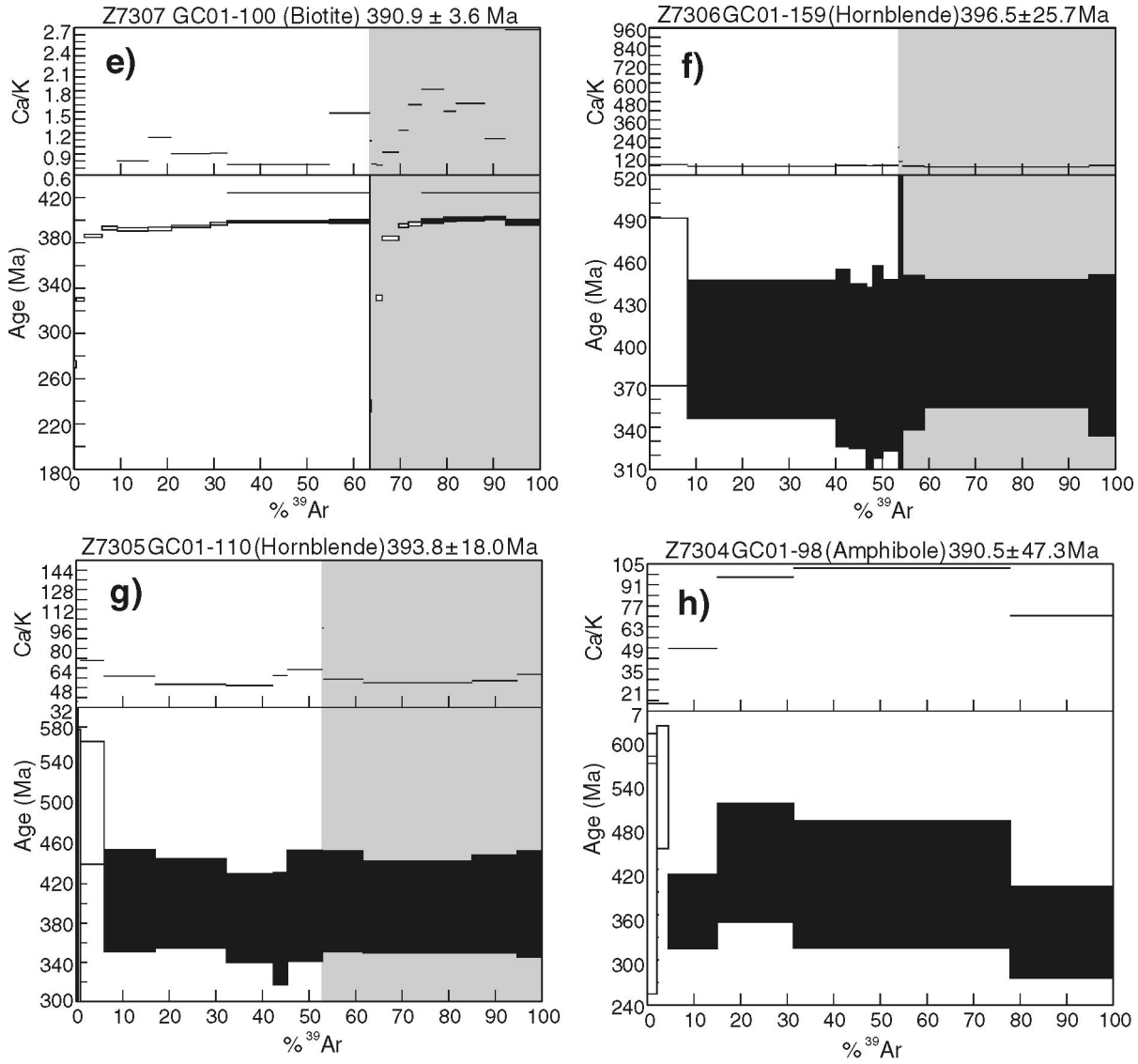

Figure 6. *(Cont.)*

GC01-98

Analysis of hornblende in this sample from relatively fresh gabbro in drill core gave a four-step plateau age of 391 ± 47 Ma. The large error is due to very low K content and small amounts of argon gas for analysis (Fig. 6h).

DISCUSSION AND CONCLUSIONS

The U-Pb and Ar/Ar ages are summarized in Table 4, and their significance for the timing of gold mineralization is discussed below.

At Clarence Stream, vein-associated mineralization is interpreted to have occurred from the late stage of, to after, the development of the regional foliation (S_3 of Castonguay et al., 2003); and prior to, or synchronous with, the deformation (boudinage) of the dykes. Based on the data reported above, a maximum age for mineralization is provided by the ca. 400 Ma age of inherited zircon grains in the boudinaged auriferous dyke, and the 395.5 ± 0.5 Ma crystallization age of a late- to post-foliation, pre-boudinage granite dyke. The latter age is identical to the reported age of 396 ± 1 Ma for the adjacent Magaguadavic phase of the St. George Batholith (Bevier, 1990). The 395 Ma date must be considered a maximum age for the mineralizing event as no minimum age on the timing of boudinage and D_3 shear zone development has been determined.

The three muscovite samples yield a range in age from 395 to 388 Ma that statistically do not define a single age population, possibly indicating different cooling or crystallization events. Minimum age estimates for the timing of mineralization are provided by $^{40}Ar/^{39}Ar$ muscovite ages from mineralized aplitic dyke and sulphide-bearing quartz veins at 395 ± 3.6 Ma and 389 ± 4 Ma, respectively. The 395 ± 3.6 Ma muscovite age provides a direct temporal link to the age of magmatic rocks in the area, as it may represent the cooling age below the estimated argon closure temperatures of 350ºC for muscovite. The younger ages for samples GC01-148 and GC01-095 may be interpreted in one of two ways: 1) they represent cooling following vein emplacement or overprinted ages following initial crystallization within the dykes at ca. 395 Ma; or 2) they represent a hydrothermally driven recrystallization and fluid activity at ca. 390 Ma, perhaps associated with remobilization of the mineralizing system. It is notable that if the latter is the case, the younger ages overlap within error of the date for youngest intrusions associated with the South Oromocto Lake Intrusive Suite (the John Lee Brook Granite: 384 +/-± 7 Ma).

These possibilities remain difficult to assess without a good estimate of the age of regional metamorphism in the Clarence Stream area. Hornblende analyses are imprecise owing to low potassium contents, and yield a weighted mean age of 394 ± 14 Ma, consistent with a metamorphism broadly contemporaneous with intrusion of the Magaguadavic phase of the Saint George Batholith. A more precise result for metamorphic biotite from a gabbro gives an age of 390.9 ± 3.6 Ma, identical to the muscovite ages. The low closure temperature for biotite would be expected to yield slightly younger ages in

Table 4. Summary of Ar-Ar and U-Pb age results, SW New Brunswick TGI area.

Sample	Lab #	Mineral	Rock Type	Field Interpretation	Age interprtetation	^{40}Ar-^{39}Ar Result		U-Pb Result	
						Age(Ma)	± 2 σ	Age (Ma)	± 2 σ
GC01-165	7186	muscovite	Aplite	syn-mineralization	plateau	395.6	3.6	-	-
GC01-148	7187	muscovite	Quartz vein post hornfels	post-contact metamorphism	plateau	388.8	3.6	-	-
GC01-95	7308	muscovite	metasedimentary	metamorphism	plateau	389.3	3.5	-	-
								-	-
GC01-159	7306	amphibole	Gabbro	metamorphsim	plateau	397	26	-	-
GC01-100	7307	biotite	Gabbro	thermal metamorphsim	plateau	390.9	3.6	-	-
GC01-110	7305	amphibole	Gabbro	metamorphsim	plateau	394	18	-	-
GC01-98	7304	amphibole	Gabbro	metamorphsim	plateau	391	47	-	-
GC01-163	7302	monazite, biotite	Granite	crystallization age	wt avg. 207Pb/235U	no age	-	395.5	0.5
GC01-146	7084	zircon, titanite	Jimmy Hill Granite	crystallization age	zircon upper intercept age	-	-	403.0	2.0
Kedrin 01	7531	monazite, thorite	Kedrin Granite	alteration	wt avg. 207Pb/235U	-	-	313.0	4.0
02SC-055	7530	zircon	Tower Hill microgranite	pre-mineralization	zircon concordia	-		409.0	1.0
GC01-150	7085	zircon	Mineralized pegmatite	age of inherited grains;	SHRIMP 206Pb/238U ages	-	-	400.0	5.0

relatively slowly cooled domains. If peak metamorphism occurred at ca. 395 Ma, then cooling through muscovite and biotite closure (350ºC–250ºC) occurred relatively soon after 391 Ma. In a geochronological study of gold mineralization in the Tintina gold belt, Alaska, Selby et al (2002) pointed out that $^{40}Ar/^{39}Ar$ ages of muscovite in vein selvages are approximately 4 Ma younger than the interpreted age of sulphide mineralization and magmatism as determined by Re-Os and U-Pb age dating. The 390 Ma $^{40}Ar/^{39}Ar$ ages reported here may similarly represent minimum ages of mineralization.

The timing of mineralization at other locations reported here is less precisely constrained, but is broadly consistent with the results at Clarence Stream. At the Tower Hill occurrence, mineralization must postdate 409 ± 2.4 Ma, the age of a mineralized microgranite dyke. No firm constraints are available at Jimmy Hill, other than establishing a spatial association with a Devonian plutonic phase of the South Oromocto Lake Intrusive Suite at 403 ± 2 Ma. The only indication of younger activity in this study is the 313 Ma age for monazite from the Kedron pluton. The monazite from this sample is interpreted to indicate a metamorphic or hydrothermal origin, and postdates intrusion of the pluton, best estimated at ca. 360 Ma. The timing of monazite growth in the sample is broadly contemporaneous with mid-Carboniferous faulting along the Avalon-Meguma boundary (e.g. Waldron et al., 1989; Calder, 1998), and the data are interpreted to indicate fluid activity associated with the Alleghanian deformation events. This fluid activity likely did not play a significant role in the gold mineralization associated with the Kedron pluton since the endocontact mineralized zone, at least, is very similar to those prolifically developed during Late Devonian time at the nearby Mount Pleasant mine . Regionally, however, there is mounting evidence for widespread and possibly significant auriferous hydrothermal activity during mid-Carboniferous time elsewhere in southern New Brunswick (Johnson and Gardiner, 2003), the age of which may be, in part, indicated by the young date.

In conclusion, the new age data reported here for gold occurrences in southwestern New Brunswick reinforce proposals that gold mineralization in southwestern New Brunswick is spatially and temporally association with Early Devonian plutonic phases of the Saint George Batholith. Although the new ages reported from the Clarence Stream area indicate an important Early Devonian mineralization, minor gold mineralization is locally associated with Late Devonian (ca. 360 Ma) magmatic rocks in the area.

ACKNOWLEDMENTS

We thank Kay Thorne and Leslie Fyffe, from the New Brunswick Department of Natural Resources and Energy, and David Lentz, University of New Brunswick, for helpful discussion on regional and local geology. Many thanks to Freewest Resources Inc. (Don Hoy, Glen Lutes, and George Murphy) for their support and for allowing unlimited access to their property, drill cores and various datasets. Xueming Yang (UNB) assisted in sample collection (GC01-163). Sheila Watters collected sample Kedron-01. Julie Peressini, Dianne Bellerive, Carole Lafontaine, and Nancy Joyce provided analytical support. Vicki McNicoll is thanked for her helpful review.

REFERENCES

Bevier, M.L.
1989 : U-Pb geochronologic studies of igneous rocks in New Brunswick; New Brunswick Department of Natural Resources and Energy, Minerals and Energy Division, Information Circular 88-2, p. 134–140.
1990: Preliminary U-Pb geochronologic results for igneous and metamorphic rocks, New Brunswick; *in* Project Summaries for 1989, Fourteenth Annual Review of Activities, (ed.) S. A. Abbott; New Brunswick Department of Natural Resources and Energy Division, Information Circular 89-2 (Second Edition), p. 208–212.

Calder, J.H.
1998: The Carboniferous evolution of Nova Scotia: *in* Lyell; the past is the key to the present, (ed) D.J. Blundell and A.C. Scott; Geological Society of London, Special Publication 143; p. 261–302.

Castonguay, S., Watters, S., and Ravenelle, J.-F.
2003: Preliminary report on the structural geology of the Clarence Stream–Moores Mills area, southwestern New Brunswick: implications for gold exploration; Geological Survey of Canada, Current Research 2003-D2, 10 p.

Chi, G.
2002: Fluid compositions and temperature-pressure conditions of intrusion-related gold systems in southwestern New Brunswick — a fluid inclusion study; Geological Survey of Canada, Current Research 2002-E13, 11 p.

Chi, G., Watters, S., Davis, W., Fyffe, L.R., McLeod, M.J., Lentz, D.R., Yang, X., Thorne, K., Castonguay, S., Tremblay, A., Dubé, B., Savard, M.M., Johnson, S., Lauzière, K., Rennick, P., and Hoy, .
2001: Metallogeny of intrusion-related gold systems in southwestern New Brunswick; New Brunswick Department of Natural Resources and Energy, Minerals and Energy Division, Abstracts, 2001: 26th Annual Review of Activities, p. 15–16.

Cumming, G.L. and Richards, J.R.
1975: Ore lead in a continuously changing Earth; Earth and Planetary Science Letters, v. 28, p. 155–171.

Davis, W.J., McNicoll, V.J., Bellerive, D.R., Santowski, K. and Scott, D.J.
1997: Modified chemical procedures for the extraction and purification of uranium from titanite, allanite and rutile in the Geochronology Laboratory, Geological Survey of Canada; *in* Radiogenic Age and Isotopic Studies: Report 10, Geological Survey of Canada, Current Research 97-F, p. 33 5.

Fyffe, L.R. and Brown, D.F.,
1996. Petrographic examination of the otter lake drill holes, Charlotte County, New Brunswick; *in* Current Research 1995, (ed.) B..M.W. Carroll; New Brunswick Department of Natural Resources and Energy, Minerals and Energy Division, Mineral Resource Report 96-1, p. 1–12.

Fyffe, L.R. and Fricker, A.
1987: Tectonostratigraphic terrane analysis of New Brunswick; Maritime Sediments and Atlantic Geology, v. 23, p. 113–123.

Fyffe, L.R. and Thorne, K.G
2002: Geology of the Clarence Stream area (NTS 21 G/07d), Charlotte County, New Brunswick; New Brunswick Department of Natural Resources and Energy, Minerals, Policy and Planning Divison, Plate 2002-52, scale 1:20 000.

Fyffe L.R., Pickerill, R.K., and Stringer, P.
1999: Stratigraphy, sedimentology and structure of the Oak Bay and Waweig formations, Mascarene Basin: implications for the paleotectonic evolution of southwestern New Brunswick; Atlantic Geology, v. 35, p. 59–84.

Johnson, S.C. and Gardiner, W.W.
2003: Conceptual models and potential gold models in the Carboniferous rocks of New Brunswick; *in* Abstracts, 2003: 28th Annual Review of Activities, (ed.) B.M.W. Carroll; New Brunswick Department of Natural Resources, Information Circular 2003-1, p. 23–24.

Krogh, T.E.
1982: Improved accuracy of U-Pb ages by the creation of more concordant systems using an air abrasion technique; Geochimica et Cosmochimica Acta, v. 46, p. 637 49.
Lang, J.R. and Baker, T.
2001: Intrusion-related gold systems: the present level of understanding; Mineralium Deposita, v. 36, p. 477–489.
Ludman, A.
1991: Revised stratigraphy of the Cookson Group in eastern Maine and southwestern New Brunswick: an alternate view; Atlantic Geology, v. 27, p. 49–55.
Ludwig, K.R.
2001: User's manual for Isoplot/Ex rev. 2.49: a geochronological toolkit for Microsoft Excel, Berkeley Geochronology Center, Special Publication 1a, , Berkeley, California, 55 p.
McLeod, M.J.
1990: Geology, geochemistry, and related mineral deposits of the Saint George Batholith, Charlotte, Queens, and Kings Counties, New Brunswick; New Brunswick Department of Natural Resources and Energy, Mineral Resource Report 5, 169 p.
McLeod, M.J. and Fyffe L.R.
2002: Geology and gold occurrences, Clarence Stream area, southwestern New Brunswick; New Brunswick Department of Natural Resources and Energy, Minerals and Energy Division, Plate 2002-38A, scale 1:100 000.
McLeod, M.J. and McCutcheon, S.R.
2000: Gold environments in New Brunswick; New Brunswick Department of Natural Resources and Energy, Minerals and Energy Division, Plate 2000-8.
McLeod, M.J., Johnson, S.C., and Ruitenberg, A.A.
1994: Geological map of southwestern New Brunswick; New Brunswick Department of Natural Resources and Energy, Mineral Resources, Map NR-5, scale 1:250 000.
McLeod, M.J., Taylor, R.P., and Lux, D.R.
1988. Geology, $^{40}Ar/^{39}Ar$ geochronology and Sn-W-Mo-bearing sheeted veins of the Mount Douglas Granite, southwestern New Brunswick; Canadian Mining and Metallurgical Bulletin, v. 81, No. 918, p. 70–77.
Miller, B.V. and Fyffe, L.R.
2002. Geochronology of the Letete and Waweig formations, Mascarene Group, Southwestern New Brunswick; Atlantic Geology, v. 38, p. 29–36.
New Brunswick Department of Natural Resources and Energy
2000: Bedrock geology of New Brunswick, Map NR-1, scale 1:500 000.
Parrish, R.R., Roddick, J.C., Loveridge, W.D., and Sullivan, R.W.
1987: Uranium-lead analytical techniques at the geochronology laboratory, Geological Survey of Canada; *in* Radiogenic Age and Isotopic Studies: Report 1, Geological Survey of Canada, Paper 87-2, p. 3–7.
Renne, P.R., Deino, A.L., Walter, R.C., Turrin, B.D., Swisher, C.C., III, Becker, T.A., Curtis, G.H., Sharp, W D. and Jaouni, A.R.
1994: Intercalibration of astronomical and radioisotopic time; Geology, v. 22, p. 783–786.
Roddick, J.C.
1987: Generalized numerical error analysis with applications to geochronology and thermodynamics; Geochimica et Cosmochimica Acta, v. 51, no. 8, p. 2129 135.
1988: The assessment of errors in $^{40}Ar/^{39}Ar$ dating; *in*: Radiogenic Age and Isotopic Studies, Report 2; Geological Survey of Canada, Paper 88-2, p. 7–16.
Roddick. J.C., Loveridge, W.D., Parrish, R.R.
1987: Precise U Pb dating of zircon at the sub-nanogram Pb level; Chemical Geology, v. 66, p. 111–121.
Ruitenberg, A.A.
1967: Stratigraphy, structure and metallization Piskahegan-Rolling Dam area, northern Appalachians, New Brunswick, Canada; Leidse Geologische Mededelingen, v. 40, p. 79–120.
1972: Metallization episodes related to tectonic evolution, Rolling Dam and Mascarene-Nerepis Belts, New Brunswick; Economic Geology, v. 67, p. 434-444.
Scharer, U.
1984: The effect of initial (super 230) Th disequilibrium on young U-Pb ages; the Makalu case, Himalaya. Earth and Planetary Science Letters, 67: 191-204.
Selby, D., Creaser, R.A., Hart, C.J.R., Rombach, C.S., Thompson, J.F.H., Smith, M.T., Bakke, A.A., and Goldfarb, R.J.
2002: Absolute timing of sulfide and gold mineralization; a comparison of Re-Os molybdenite and Ar-Ar mica methods from the Tintina gold belt, Alaska; Geology, v. 30, p. 791–794.Seal, R.R., Clark, A.H., and Morrissy, C.J.
1988. Lake George, southwestern New Brunswick: a Silurian, multi-stage, polymetallic (Sb-W-Mo-Au-base metal) hydrothermal centre; *in* Recent Advances in the Geology of Granite-Related Mineral Deposits, (ed.) R.P. Taylor and D.F. Strong; Canadian Institute of Mining and Metallurgy Conference on Granite-Related Mineral Deposits, September 15–17, 1985, Halifax, Nova Scotia, Special Volume 39, p. 252-264.
Sinclair, W.D., Kooiman, G.J.A., and Martin, D.A.
1988: Geological setting of granites and related tin deposits in the North Zone, Mount Pleasant, New Brunswick; *in* Current Research, Part B, Geological Survey of Canada, Paper 88-1B, p. 201–208.
Stern, R.A.
1997: The GSC Sensitive High Resolution Ion Microprobe (SHRIMP): analytical techniques of zircon U-Th-Pb age determinations and performance evaluation; *in* Radiogenic Age and Isotopic Studies, Report 10, Geological Survey of Canada, Current Research 1997-F, p. 1–31.
Stern, R.A. and Amelin, Y.
2003: Assessment of errors in SIMS zircon U-Pb geochronology using a natural zircon standard and NIST SRM 610 glass; Chemical Geology, v. 197, p. 111–146.
Taylor, R.P.
1992. Petrological and geochemical characteristics of the Pleasant Ridge zinnwaldite-topaz granite, southern New Brunswick, and comparisons with other topaz-bearing felsic rocks; Canadian Mineralogist, v. 30, p. 895–921.
Taylor, R.P., Sinclair, W.D., and Lutes, G.
1985: Geochemical and isotopic characterization of granites related to W-Sn-Mo mineralization in the Mount Pleasant area, New Brunswick; *in* Granite-Related Mineral Deposits, Geology, Petrogenesis and Tectonic Setting, Extended abstracts of Papers, (ed.) R.P. Taylor and D.F. Strong**;** Sanadian Institute of Mining aod Metallurgy Conference on Granite-Related Mineral Deposits, Halifax, Canada, September 15–17, 1985, p. 265–273.
Thomas, M.D. and Willis, C.
1989: Gravity modeling of the Saint George Batholith and adjacent terrane within the Appalachian Orogen, southern New Brunswick; Canadian Journal of Earth Sciences, v. 26, p. 561–576.
2003: Geology of the Main Zone of the Clarence Stream deposit, southwestern New Brunswick; *in* Gold Deposits Associated With Felsic Intrusions in Southwestern New Brunswick — Field Guidebook, (ed.) K. Thorne and M. McLeod; New Brunswick Department of Natural Resources and Energy, Minerals, Policy and Planning Division, Open File 2003-4, p.59–64.
Thorne, K. and McLeod, M.J. (ed.)
2003a: Gold deposits associated with felsic intrusions in southwestern New Brunswick — Field Guidebook; New Brunswick Department of Natural Resources and Energy; Minerals, Policy and Planning Division, Open File 2003-4, 83 p.
2003b: Kedron gold occurrence, northern Saint George Batholith, southwestern New Brunswick;. *in* Gold Deposits Associated With Felsic Intrusions in Southwestern New Brunswick — Field Guidebook, (ed.) K. Thorne and M. McLeod; New Brunswick Department of Natural Resources and Energy, Minerals, Policy and Planning Division, Open File 2003-4, p.31–33.
Thorne, K. and Ravenelle, J-F
2003: Tower Hill gold occurrence, southwestern New Brunswick; *in* Gold Deposits Associated With Felsic Intrusions in Southwestern New Brunswick – Field Guidebook; (ed) K. Thorne and M. McLeod; New Brunswick Department of Natural Resources and Energy, Minerals, Policy and Planning Division, Open File 2003-4, p.59–64.
Thorne, K.G., Hoy, D., and Lentz, D.R.
2001: Field guidebook: the Clarence Stream gold deposit, southwestern New Brunswick; New Brunswick Department of Natural Resources and Energy, Mineral and Energy Division, Open File 2001-9, 16 p.
Thorne, K.G., Lentz, D.R., Hall, D.C., and Yang, X.M.
2002a: Petrology, geochemistry, and geochronology of the granitic pegmatite and aplite dykes associated with the Clarence Stream gold deposit, southwestern New Brunswick; Geological Survey of Canada, Current Research 2002-E12, 13 p.

Thorne, K.G., Lutes, G.G., and Fyffe, L.R.
2002b: Geology of the West and Central zones, Clarence Stream gold deposit, Charlotte County, New Brunswick; New Brunswick Department of Natural Resources and Energy; Minerals, Policy and Planning Division, Plate 2002-54B, scale 1: 1000.
2002c: Geology of the East Zone, Clarence Stream gold deposit, Charlotte County, New Brunswick; New Brunswick Department of Natural Resources and Energy; Minerals, Policy and Planning Division, Plate 2002-54A, scale 1: 1000.

Villeneuve, M.E. and MacIntyre, D.G
1997: Laser $^{40}Ar/^{39}Ar$ ages of the Babine porphyries and Newman Volcanics, Fulton Lake map area, west-central British Columbia; *in* Radiogenic Age and Isotopic Studies, Report 10; Geological Survey of Canada, Current Research 1997-F, p.131–139.

Villeneuve, M.E., Sandeman, H.A., and Davis, W.J.
2000: A method for the intercalibration of U-Th-Pb and $^{40}Ar/^{39}Ar$ ages in the Phanerozoic; Geochimica et Cosmochimica Acta, v. 64, p. 4017–4030.

Waldron, J.W.F, Piper, D.J.W., and Pe-Piper, G.
1989: Deformation of the Cape Chignecto Pluton, Cobequid Highlands, Nova Scotia: thrusting at the Meguma-Avalon boundary; Alantic Geology, v. 25, p. 51—62.

Watters, S., Castonguay, S., and McLeod, M.J.
2003: Preliminary report on new gold deposits in the Clarence Stream area of southern New Brunswick: Anomaly "A" —distal deposits of an intrusion-related gold system?; Geological Survey of Canada, Open File 1779, 40 p.

Williams, H.
1995: Temporal and spatial divisions; Chapter 2 *in* Geology of the Appalachians-Caledonian Orogen in Canada and Greenland. (ed.) H. Williams; Geological Survey of Canada, Geology of Canada, no. 6, p. 21–44 (also Geological Society of America, The Geology of North America, v.F-1, P.21–44).

York, D.
1969: Least squares fitting of a straight line with correlated errors; Earth and Planetary Science Letters; v. 5, p. 320–324.

Appendix A. Analytical Techniques

U-Pb thermal ionization mass spectrometry (TIMS)

Heavy mineral concentrates were prepared by standard techniques (crushing, grinding, Wilfley^{TM} table, heavy liquids), and sorted by magnetic susceptibility using a Frantz^{TM} isodynamic separator. All zircon and titanite fractions were air abraded (Krogh,1982). Monazite and thorite fractions were not abraded. Analytical methods for U-Pb TIMS analyses of zircon and monazite are summarized in Roddick et al. (1987) and Parrish et al. (1987), and for titanite in Uranium and lead isotopic compositions were determined in static mode using a Finnigan Mat 261 mass spectrometer. Samples were collected for common lead assuming an analytical blank of 3-8 pg with the composition listed in Table 1. The ^{233}U-^{235}U-^{205}Pb spike was calibrated against gravimetric standard solutions to better than 0.2% (2SE). Analytical errors are determined based on error propagation methods of Roddick (1987). Analytical results are presented in Table 1 and Figure 2. A modified regression method (York, 1969) was used to calculate upper and lower concordia intercept ages.

U-Pb sensitive high-resolution ion microprobe (SHRIMP)

SHRIMP analytical procedures followed those described by Stern (1997), with standards and U-Pb calibration methods following Stern and Amelin (2003). Zircons were cast in 2.5 cm diameter epoxy mounts along with fragments of the GSC laboratory standard zircon (z6266, with $^{206}Pb/^{238}U$ age = 559 Ma). The midsections of the zircons were exposed using 9, 6, and 1 µm diamond compound, and the internal features of the zircons (such as zoning, structures, alteration, etc.) were characterized with backscattered electrons (BSE) utilizing a Cambridge Instruments scanning electron microscope. Mount surfaces were evaporatively coated with 10 nm of high purity gold. Analyses were conducted using an $^{16}O^-$ primary beam, projected onto the zircons at 10 kV. The count rates of ten isotopes of Zr^+, U^+, Th^+, and Pb^+ in zircon were sequentially measured with a single electron multiplier and a pulse-counting system with deadtime of 28 ns. Mass resolution was approximately 5000 (1%). Off-line data processing was accomplished using customized in-house software. The 1σ external errors of $^{206}Pb/^{238}U$ ratios reported in Table 2 incorporate a ±1.0 % error in calibrating the standard zircon (*see* Stern and Amelin, 2003). No fractionation correction was applied to the lead-isotope data; common lead correction utilized the measured $^{204}Pb/^{206}Pb$ and compositions modelled after Cumming and Richards (1975). Isoplot v. 2.49 (Ludwig, 2001) was used to generate concordia plots and calculate weighted means.

$^{40}Ar/^{39}Ar$ methods

Selected samples were processed for $^{40}Ar/^{39}Ar$ analysis by standard mineral-separation techniques, including hand-picking of clear, unaltered crystals. Individual mineral separates were loaded into aluminium foil packets along with a single grain of Fish Canyon Tuff Sanidine (FCT-SAN) to act as flux monitor (apparent age = 28.03 ± 0.1 Ma; Renne et al., 1994). The sample packets were arranged radially inside an aluminium can. The samples were then irradiated for 12 hours at the research reactor of McMaster University in a fast neutron flux of approximately $3x10^{16}$ neutrons/cm^2.

Laser $^{40}Ar/^{39}Ar$ step-heating analysis was carried out at the Geological Survey of Canada laboratories in Ottawa, Ontario. Upon return from the reactor, samples were split into several aliquots and loaded into individual 1.5 mm diameter holes in a copper planchet. The planchet was then placed in the extraction line and the system evacuated. Heating of individual sample aliquots in steps of increasing temperature was achieved using a Merchantek MIR10 10W CO_2 laser equipped with a 2 mm x 2 mm flat-field lens. The released Ar gas was cleaned over getters for ten minutes, and then analyzed isotopically using the secondary electron multiplier system of a VG3600 gas source mass spectrometer; details of data collection protocols can be found in Villeneuve and MacIntyre (1997) and Villeneuve et al. (2000).

Corrected argon isotopic data are listed in Table 3. Some gas-release spectra plotted contain step-heating data from two or more aliquots, alternately shaded and normalized to the total volume of ^{39}Ar released on Figure 6. Such plots provide a visual image of replicated heating profiles, evidence for argon loss in the low-temperature steps, and the error and apparent age of each step.

Neutron flux gradients throughout the sample canister were evaluated by analyzing the sanidine flux monitors included with each sample packet and interpolating a linear fit against calculated J-factor and sample position. The error on individual J-factor values is conservatively estimated at ±0.6% (2σ). Because the error associated with the J-factor is systematic and not related to individual analyses, correction for this uncertainty is not applied until calculation of dates from isotopic correlation diagrams (Roddick, 1988). No evidence for excess ^{40}Ar was observed in any of the samples and, therefore, all regressions are assumed to pass through the $^{40}Ar/^{36}Ar$ value for atmospheric air (295.5). All errors are quoted at the 2σ level of uncertainty.